HAVA VE UYDU PLATFORMLARINDAN ALINAN GÖRÜNTÜLERDEN BİTKİ ÖRTÜSÜ ÇIKARIMI VE İZLENMESİ

VEGETATION COVER EXTRACTION AND MONITORING USING IMAGES OBTAINED FROM AERIAL AND SATELLITE PLATFORMS

ÖMER KANTARCIOĞLU

ASSOC.PROF.DR. SULTAN KOCAMAN GÖKÇEOĞLU

Supervisor

Submitted to

Graduate School of Science and Engineering of Hacettepe University

as a Partial Fulfillment to the Requirements

for the Award of Degree Master of Science

in Geomatics Engineering.

2021

ÖZET

HAVA VE UYDU PLATFORMLARINDAN ALINAN GÖRÜNTÜLERDEN BİTKİ ÖRTÜSÜ ÇIKARIMI VE İZLENMESİ

Ömer KANTARCIOĞLU

Geomatik Mühendisliği Yüksek Lisans

Tez Danışmanı: Doç. Dr. Sultan KOCAMAN GÖKÇEOĞLU

Haziran 2021, 65 sayfa

Bitki örtüsü, kentsel ısı adası etkisinin azaltılması, ekolojik dengenin sürdürülmesi, biyolojik çeşitliliğin korunması, yaşam kalitesinin iyileştirilmesi vb. gibi birçok açıdan hem kentsel hem de kırsal ortamlarda önemli bir role sahiptir. Farklılıkları ayırt etmek için görüntü işleme yöntemleri kullanılarak bitki örtüsü değişikliği tespiti yapılabilir. Bunun için farklı zamanlarda çekilen görüntülerin kullanılması gerekmektedir. Kentsel alanlarda bitki örtüsü değişikliği, şehirlerin yeşil altyapısının büyüme veya azalması açısından iyi bir gösterge olabilir. Diğer yandan, kırsal alanlardaki değişim, tarım alanlarının büyümesi veya azalması anlamına gelebilir. Bu tez çalışması, farklı mevsim ve yıllarda hava ve uydu sensörlerinden elde edilen çok zamanlı ve çok platformlu verileri kullanarak bitki örtüsü değişikliği tespit yöntemlerini araştırmayı amaçlamıştır. İnsansız Hava Araçlarına (İHA) monte edilen RGB kameralardan ve çok bantlı Yer Gözlem (EO)

uydu sensörlerinden (Göktürk-1 ve Worldview-2) alınan görüntüler bu çalışmada veri kaynağı olarak kullanılmıştır. Çalışma alanı, veri mevcudiyeti dikkate alınarak Antalya Akdeniz Üniversitesi Kampüsü'nde yer alan koruluk bölgeden seçilmiştir. Radyometrik ve geometrik iyileştirmeler için yapılan bir dizi görüntü ön işleme yöntemi, değişiklik tespitinden önceki ilk adımları oluşturmaktadır. Görüntülerin doğru yöneltilmesi için farklı jeoreferanslama yöntemleri uygulanmıştır. Normalleştirilmiş bitki örtüsü farklılık indeksi (NDVI) ve Yeşil ve Kırmızı Oran Bitki Örtüsü İndeksi (GRVI) gibi çeşitli bitki örtüsü indeksleri, bitki örtüsünü daha iyi tanımlamak için veri setlerinden türetilmiştir. NDVI ve GRVI görüntüleri, bitki örtüsü sınıflandırması için denetimli bir makine öğrenimi (MÖ) yöntemi olan rastgele orman (RO) metodu kullanılmıştır. Doğrulama sonuçları, RO yönteminin çoklu-zamanlı, çoklu-çözünürlüklü ve çoklu-platformlu veri kümeleri için bitki örtüsü haritalaması ve karar seviyesinde değişiklik tespiti için uygun bir yöntem olduğunu göstermektedir. Ayrıca, denetimsiz bitki örtüsü haritalaması amaçlı olarak bu tezde kullanılan tüm sensörlerden elde edilen GRVI verilerine Otsu eşik-değer yöntemi uygulanmış ve başarılı sonuçlar ürettiği görülmüştür.

Anahtar Kelimeler: Bitki örtüsü haritalama, Görüntü İşleme, İnsansız Hava Araçları, Optik Uydu Görüntüleri, Değişim Belirleme, Worldview-2, Göktürk-1.

ABSTRACT

VEGETATION COVER EXTRACTION AND MONITORING USING IMAGES OBTAINED FROM AERIAL AND SATELLITE PLATFORMS

Omer KANTARCIOGLU

Master of Science, Department of Geomatics Engineering

Supervisor: Assoc. Prof. Dr. Sultan KOCAMAN GÖKÇEOĞLU

June 2021, 65 pages

Vegetation cover has an essential role in both urban and rural environments in several aspects, such as mitigating urban heat island effect, sustaining ecological balance, preserving biodiversity, improving the quality of life, etc. Vegetation change detection can be carried out by using image processing methods in order to distinguish differences. For this purpose, images taken at different moments need to be utilized. In urban areas, vegetation change can be a great indicator for the growth or decrease of cities green infrastructure. In contrast, the change in rural areas could mean the growth or decrease of agricultural fields. This thesis aimed to investigate the vegetation change detection methods by using multi-temporal and multi-platform data, i.e. obtained from aerial and satellite sensors at different seasons and years. Data from RGB cameras mounted on Unmanned Aerial Vehicles (UAV), and from multispectral Earth Observation (EO) satellite sensors (i.e. Gokturk-1 and Worldview-2) have been employed as data sources

in this study. The study area was selected from the forest area in Akdeniz University Campus, Antalya, Turkey, due to data availability. A number of image pre-processing methods for radiometric and geometric improvements were the initial tasks prior to change detection. Different georeferencing methods were applied for accurate alignment of the images. Several vegetation indices such as normalized difference vegetation index (NDVI) and Green and Red ratio Vegetation Index (GRVI) were derived from the datasets to identify the vegetation better. These NDVI and GRVI images were employed in a supervised machine learning (ML) method, i.e. the random forest (RF), for vegetation classification. The validation results show that the RF method is a suitable method for vegetation mapping and decision level change detection for multi-temporal, multi-resolution and multi-platform datasets. In addition, for the purpose of unsupervised vegetation mapping, the Otsu thresholding method was found successful when applied to the GRVI data obtained from all sensors used here.

Keywords: Vegetation mapping, Image Processing, Unmanned Aerial Vehicles, Satellite Optical Images, Change Detection, Worldview-2, Göktürk-1.

ACKNOWLEDGEMENTS

First and foremost, I’d like to thank Assoc. Prof. Dr. Sultan Kocaman for supervising my thesis. Without her assistance and dedicated involvement in every step throughout the process, this thesis would have not been accomplished. I would also like to show gratitude to Assoc. Prof. Dr. Nusret Demir for assisting me with the datasets and to Gizem Karakaş for her kind help during the most difficult times.

Most importantly, none of this could have happened without my family. I'd like to thank my brothers for always being there for me and supporting me throughout this thesis. Last but least, I'd like to thank my girlfriend for always pushing my limits and lifting me whenever I felt like giving up. None of this could have happened without having them in my life. I'd like to thank you all and I will be forever grateful.

TABLE OF CONTENTS

LIST OF FIGURES

LIST OF TABLES

ABBREVIATIONS

CD: Change Detection

DEM: Digital Elevation Model

DSM: Digital Surface Model

DTM: Digital Terrain Model

NIR: Near Infrared

RGB: Red Green Blue

UAV: Unmanned Aerial Vehicles,

RMSE: Root Mean Square Error

GK-1: Göktürk 1

WV-2: Worldview 2

HR: High Resolution

EO: Earth Observation

RF: Random Forest

SVM: Support Vector Machine

NDVI: Normalized Difference Vegetation Index

GRVI: Green-Red Vegetation Index

EVI: Enhanced Vegetation Index

DT: Decision Trees

GCP: Ground Control Point

ML: Machine Learning

DL: Deep Learning

CNN: Convolutional Neural Networks

VHR: Very High Resolution

UHR: Ultra High Resolution

1. INTRODUCTION

1.1 Vegetation Mapping and Change Detection

Vegetation cover has an essential role in urban environments in several aspects, e.g., mitigating urban heat island effect, sustaining ecological balance, preserving biodiversity, improving the quality of life, etc. Vegetation mapping includes the determination of the spatial distributions various plant species; and is crucial for analyzing vegetation dynamics, quantifying spatial patterns of vegetation development, examining the outcomes of environmental variations, and predicting spatial patterns of species diversity. Satellite imagery and aerial photography are useful data sources for observing vegetation both in urban and rural areas. In general, spatial resolutions of images utilized for vegetation mapping in cities can be diverse. The images used for this purpose can be moderate or high resolution (HR), and even very HR (VHR). In addition, images obtained from unmanned aerial vehicle (UAV) platforms can be ultra-high resolution (UHR) [1].

The earth surface is dynamic, and the changes may source from disasters, deforestation, dislocation in course of river, urbanization etc. The changes on earth surface can be classified into two groups, i.e. land use and land cover (LULC). The land use explains the actual use type of land, e.g., agriculture, urbanization, mining, etc. The land cover includes visually observable objects on the Earth's surface, such as buildings, pavement, trees etc. The change detection (CD) methods aim to distinguish differences on Earth's surface and often images taken at different moments are used for this purpose.

The CD applications employ multi-temporal datasets to quantitatively assess the changes of land cover properties. The CD activities can be performed by traditional manual observations, or by using remote sensing data and applying automated or semi-automated techniques. The manual methods are costly, time-consuming, and may possibly be inaccurate depending on the observer's skills. In addition, accessibility to the site. Thus, remote sensing data and methods can be preferred to determine the changes over large areas with high temporal frequency.

1.2 Problem Statement

In the last years, with the availability of HR remotely sensed imagery, detecting and counting trees automatically with high geolocation and semantic accuracy have become possible. Thanks to the rapid data acquisition with the remote sensing sensors, in particular the optical ones, quick assessment of forest areas and individual tree species and detecting the changes in their geometries and the other physical features, e.g. size, shape, health, etc. have been widely used by respective authorities and researchers. There is yet a growing need for reliable and cost-effective methods for operational and strategic applications such as climate change monitoring, environmental sustainability, and forest conservation.

The geometric properties of the changes in vegetated areas can be detected by numerous approaches, such as counting trees and comparing with the previous state, observing areal and volumetric changes, determination of tree decrements (e.g., deforestation), etc. Unlike the manual ground-based data collection techniques, which are time-consuming and inefficient; the remote sensing data and methods can be utilized for efficient monitoring. Often, multi-platform and multi-sensor data are needed for this purpose due to the availability of the sensor data (e.g., discontinuation of an Earth Observation (EO) satellite), practicality of multiple sensors, such as the use of different cameras mounted on UAVs, the spatial and temporal resolution requirements, etc. The spatial, spectral and radiometric resolution differences as well as the variances in data quality (e.g., geolocation accuracy) between the different sensors and platforms coupled with the physical changes in vegetated areas introduce several challenges to the vegetation monitoring problem via image CD approaches. In addition, seasonal properties and differences in image acquisition angles introduce further issues due to the illumination changes, which translate into physical changes of the vegetation in the images. Thus, the applied data and methods yield to several types of noises and unexpected errors in the resulting vegetation maps. Therefore, various techniques can be needed to be evaluated and employed for different types of image sources to obtain accurate results.

1.3 Thesis Goals

The main goal of this study was to identify vegetation in different images acquired from various platforms with multi-sensor and multi-temporal images in an urban area; and thus,

to monitor the changes over several years. The study area was selected inside Akdeniz University Campus, Antalya, Turkey due to the availability of data acquired at different years from satellite and aerial platforms (i.e., Worldview-2 satellite, UAV and Göktürk-1 satellite). An area with a size of ca. 24,000 m^2 was processed to detect the nut pine trees and to identify the changes in terms of tree count and vegetation cover. Various image processing techniques and vegetation indices were investigated in each image to exploit their potential to achieve accurate results.

The three image datasets were acquired with the sensors mentioned above; and have different spatial resolutions, acquisition conditions in terms of time of the day and the season, and other attributes such as spectral band combinations and electromagnetic spectrum bandwidths. The study aimed at investigating the different geometric preprocessing requirements for accurate alignment of the datasets; and defining an optimal processing and decision-making method for accurate mapping of the changes. Thus, a methodological approach was proposed and applied here to achieve the thesis goals.

2. RELATED WORK

2.1 Vegetation Mapping Methods

Remote sensing technologies have been developed tremendously and provide a huge amount of data for detailed analysis, detecting changes and monitoring the Earth's surface with spaceborne and airborne sensors [2]. Imagery obtained from both satellites and aerial platforms have been adopted for monitoring vegetation in urban and rural areas [3], [4]. When satellite remote sensing and aerial photogrammetry are comparatively evaluated, airborne methods have certain advantages, which make it a very dynamic field nowadays [5]. In recent works, advanced classification technologies with multi-source remote sensing images and auxiliary information are found for vegetation mapping [6]. When considering the relationship between the vegetation and the environment, many studies take advantage of auxiliary data such as elevation, soil type and precipitation, which can also improve the quality of vegetation classification [7].

Ground-based mapping is considered obsolete in many cases due to the lack of time and resource efficiency, and is leaving its place to remote sensing technologies especially in the field of vegetation mapping [8]–[13]. Even though ground-based mapping offers such precision for field surveys and detailed mapping, due to size of vegetation areas it is not often considered.

Vegetation mapping methods can broadly be categorized into unsupervised or supervised object-based and pixel-based methods. Object-oriented methods have been extensively used in vegetation mapping because of the high fragmentation and noise problem, which is also called "salt and pepper problem" that comes with the pixel-based methods [9]. In a study, a comparison was performed between the object-based methods and pixel-based methods, and the result was in favor of object-based methods by a minimal marge and achieved better spatial organization of land cover [14]. In a comparative study that evaluated the two approaches, object-based methods have yielded a higher accuracy with a difference of 15% [15]. Another study used satellite and synthetic aperture radar (SAR) data using the two methods with random forest (RF) algorithm, and superior results were achieved by the object-based approach [16]. The results obtained in [17] proved that object-based classification is more accurate and useful than pixel-based method for the

generation of vegetation maps. Another study achieved an overall accuracy of 85% using RapidEye HR satellite image with object-based classification for eight types of urban tree species [3]. A study by [18] found that the object-based approach was better for mapping crops when compared to pixel-based supervised classification methods (e.g. parallelepiped, minimum distance, Mahanalobis Distance Classifier, Spectral Angle Mapper, and MLC). Object-based methods have few disadvantages, such as the requirement of prior information of the area and the land cover type, which may not be available; and also the image segmentation and the derivation of the topological relationships between objects may yield to an overload on the computer resources and may require a large amount of memory [19].

The object-oriented methods are usually carried out in three steps. The first step is to partition the image into meaningful regions. The second step is to remove irrelevant and unnecessary features while preserving useful information to distinguish the objects based on their shape and spatial relationships. The final step is to classify the objects [4], [20]. The most important step in the object-based methods is the first one, which requires the implementation of a solid image segmentation method so that the objects are apparent to characterize the landscape for the specific objective of the work [14].

Pixel is the fundamental (spatial) unit of an image and pixel-based methods are carried out per pixel. The most commonly used pixel-based approach is supervised classification [21], in which an expert creates training areas and the algorithm assigns a label to each pixel based on the spectral signature similarity to the pre-defined training classes [21].
The machine learning (ML) methods have also been used to perform vegetation classification in remotely sensed images. The use of ML methods may improve the accuracy of remote sensing vegetation classification, but the supervised methods require a large number of samples as training data for each vegetation class [9] . Several studies based on using ML and deep learning (DL) can be found in the literature. In [22], a convolutional neural networks (CNN) architecture was used to automatically classify crops based in satellite images, and an overall accuracy of 95.9% was achieved. Another research employed DL to classify fourteen crop types while reaching an overall accuracy of 85.54% based on Landsat Enhanced Vegetation Index (EVI) times series data [23]. The studies [24], [25] adopted an artificial neural network (ANN) model for vegetation prediction and mapping.

Apart from the neural networks and the DL methods, other statistical ML methods such as RF and Support Vector Machine (SVM) have also been employed for vegetation mapping [26]. RF is a commonly used ML algorithm for handling classification and regression problems using multiple decision trees [27]. SVM is based on non-probabilistic binary linear classifiers [26]. The RF method was widely used in various studies. The researchers in [1] used the RF with UAV data for urban vegetation mapping. Another study [16] used the method with SAR data for wetland vegetation mapping. The study in [28] used it for forest habitat mapping and monitoring the ecological conditions in wetlands [8]. The study in [24] employed it for creating a HR global land cover map with Sentinel-2 satellite optical data. In [29], it was used for automated mapping for shifting cultivation. Further examples can be found in crop classification [15], [22], [23], land cover characterization and vegetation mapping in arid areas [13], [30], [31].

Vegetation Indices (VIs) have frequently been computed from multi-spectral images using various band combinations and provide useful information for many agriculture and climate studies [32]. NDVI (Normalized Difference Vegetation Index) is one of the widely used indices for vegetation classification, monitoring and rapid assessment of the vegetation quality [32]. The use of NDVI in different studies with various methods can be found in the literature [5], [29], [33].

Other than NDVI, diverse VIs, such as EVI [8], [22], [28], [34], NDYI (Normalized difference vegetation index) [28], LAI (leaf area index) [5], [25], [28], [35] and SAVI (Soil Adjusted Vegetation Index) [29], [30], [36] have been preferred in many studies. Also, NDWI (Normalized Difference Water Index) has been used for mapping wetlands [37].

2.2 Change Detection Methods in Vegetated Areas

The CD is aims at determining the differences in an area and often by using images taken at different times [38]. Another and broader definition [39] states that “in remote sensing, CD is the process that leads to the identification of changes occurred on the Earth surface by jointly processing two (or more) images acquired on the same geographical area at different times”. The changes on earth surface may occur due to disasters, deforestation, etc. [40]. Both unsupervised or supervised methods have been applied in the literature for

CD purposes [39], [41] [42]. As can be seen in the previous Section, object-based approaches overcome the problems of pixel based-methods and improve the accuracy of CD immensely [43]. The use of HR data helped to increase the accuracy of CD methods overall [44]. The CD methods can as simple as image rationing and image differencing but also including post classification and principal component analysis [40]. The CD methods have been used widely in different sectors such as forestry [45], [46], agriculture [18], urban planning [40] and water quality [47].

2.3 Integrated Use of Multi-Platform Data for Vegetation Mapping

Various remote sensing image sources are available nowadays. The high variety of camera/sensor properties provide numerous options for widely used image processing algorithms [6]. The advances in remote sensing sensors and methods have made it possible to gather information and data with high coverage of land and a great range of temporal resolution [8]. Currently, diverse satellite images are available at different temporal, spatial and spectral resolution ranges [48]. HR satellite images with high temporal resolution can be costly [49] and flying a UAV (e.g. drone) for large areas such as crops and forests can be inefficient. UAVs can obtain images at a very high spatial resolution which can be used to identify small vegetation communities, but due to logistic constraints on operating UAVs, there might be a need for using the UAV and satellite imagery together [50].

Several studies focused on using different platform in an integrated sense. Not only from a single sensor, but satellite images obtained from different sensors are also widely used to monitor the vegetation state and health [8]. Applications such as precision agriculture take advantage of using satellite imagery along with UAV data at large scales [51]. Another study [52] aimed at using both satellite imagery and UAV data while focusing on their advantages, such as the large coverage of satellite images and precise ground-truth information that comes with the UAV imagery. In a study by [53], UAV data assisted the training data collection step for SVM classification using WorldVew-3 and RapidEye satellite images together with a digital elevation model (DEM) obtained from a LiDAR (Light Detection and Ranging) sensor. In order to achieve high accuracy, an aggregate of color, texture, structure and hyperspectral properties of the UAV images were used together with the satellite imagery for the identification of invasive woody species [54]. UAVs have been used for the creation of ground-truth maps for obtaining

and generating better data than the available satellite data for treeless vegetation mapping in [55]. Fusion of Sentinel-1 SAR data and multi-spectral Sentinel-2 data was used for mapping the wetlands at the Balikdami area near Sakarya River, Turkey [56]. Also UAV and Landsat images were utilized together for orangutan habitat mapping by classifying the land cover [49].

3. STUDY AREA AND THE DATASETS

3.1 Study Area

The goal of this study was to monitor the changes over several years with images obtained from different satellite platforms and aerial platforms. The study area was selected inside Akdeniz University Campus, Antalya, Turkey, by considering the thesis goals and the availability of multi-platform images in the area (Figure 3.1). The area can be considered as a grove and mainly contains nut pine trees (Pinus Pinea) with a size of ca. 24,000 m^2. The study area can be observed through time with the data acquired from multi platforms. The first images of the area were obtained with a UAV on 10 January 2015, Worldview-2 in 7 May 2015, and Göktürk-1 images on 12 September 2019.

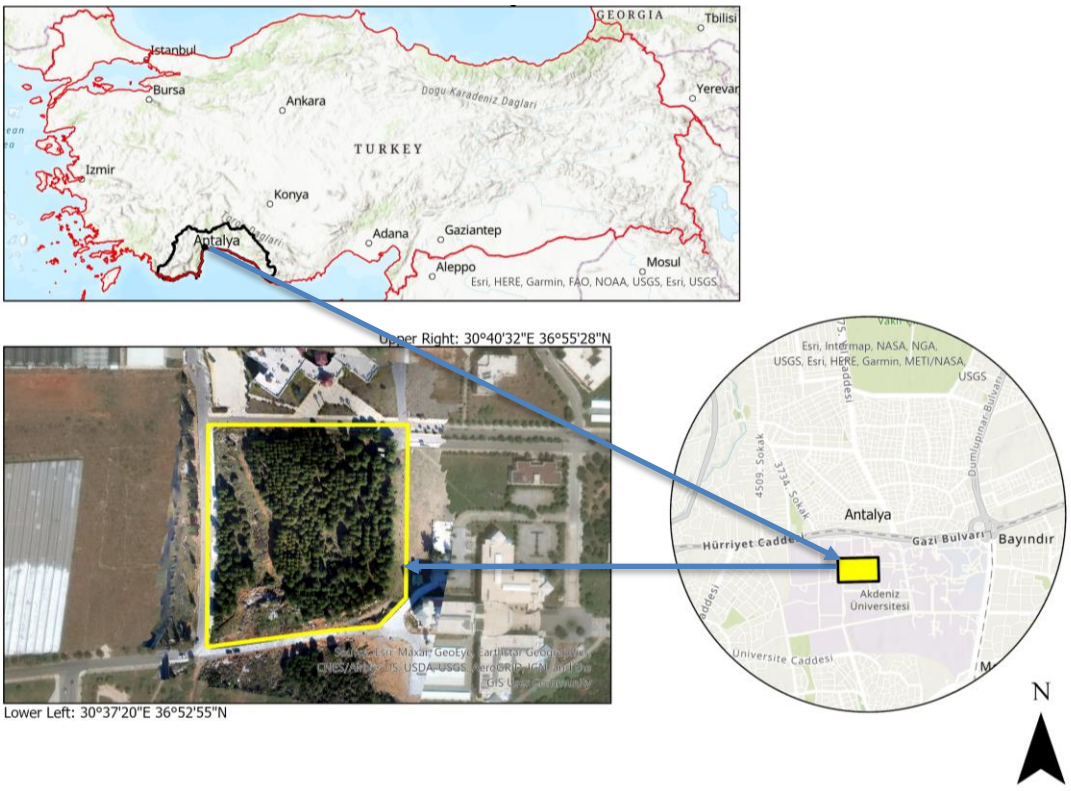

Figure 3.1: The location of the study area.

3.2 WorldView-2 Sensor & Data Characteristics

The WorldView-2 (WV-2) satellite (Figure 3.2) was launched on October 8, 2009 by United Launch Alliance (ULA). The WV-2 optical imaging sensor comprise eight multispectral (MS) bands with a spatial resolution of 2 m and a swath width of 16.4 km

at nadir. The spectral ranges of the eight bands are 400–450 nm (B1-coastal), 450–510 nm (B2-blue), 510–581 nm (B3-green), 585–625 nm (B4-yellow), 630–690 nm (B5-red), 705–745 nm (B6-red edge), 770–895 nm (B7-near infrared-1), and 860–1040 nm (B8-near infrared-2) (Table 3.1). The satellite also has a panchromatic (Pan) sensor (450–800 nm) with a nominal spatial resolution of 0.5 m [57]. According to DigitalGlobe [58] the 8 MS bands were uniquely chosen to meet the needs of a variety of applications, including resources management, coastal mapping, environmental monitoring, infrastructure mapping, and others [59].

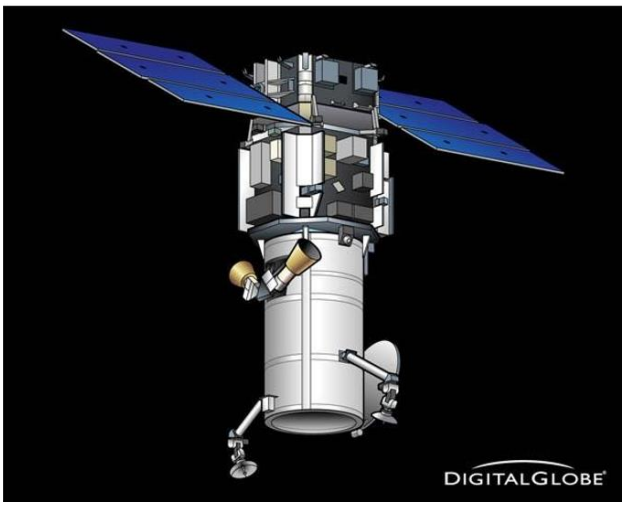

Figure 3.2. Illustration of The Worldview-2 Spacecraft (image credit: Digital Globe)

Table 3.1: WV-2 band descriptions [58]

Band Name	**Band Index**	**Spectral Characteristics(nanometers)**
Coastal	1	400-450
Blue	2	450-510
Green	3	510-580
Yellow	4	585-625
Red	5	630-690
Red Edge	6	705-745
Near IR 1	7	770-895
Near IR 2	8	860-1040
Panchromatic	-	450-800

The wavelengths of WorldView-2 bands are mainly sensitive to vegetation properties important to distinguish tree species “including 425 nm (chlorophyll absorption), 480 nm (chlorophyll absorption), 545 nm (plant health), 605 nm (carotenoid absorption detects ‘yellowness’ of vegetation), 660 nm (chlorophyll absorption), 725 nm (vegetation health), 835 nm and 950 nm(leaf mass and moisture content)” [59],[60]. The WV-2 relative spectral radiance response is depicted in Figure 3.3. Further specifications of the WV-2 satellite and the imaging instrument are given in Table 3.2.

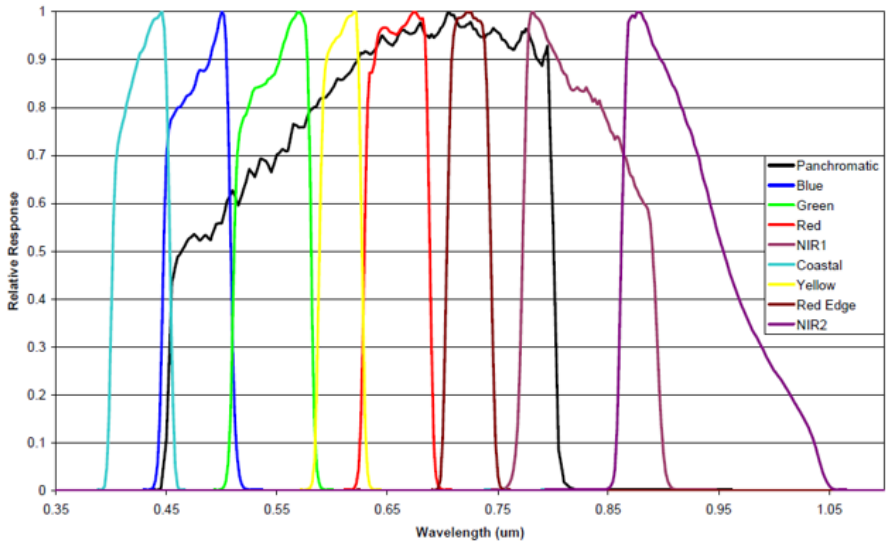

Figure 3.3: WorldView-2 relative spectral radiance response [62]

The WV-2 imagery used in this study was acquired on the 7th of May 2015. The imagery bundle received from DigitalGlobe included the Pan band image and 4 MS band (RGB + NIR) data. The dynamic range of the sensor is 11 bits and the cloud cover is 3%. Further information on the data characteristics are presented in Table 3.2. An overview of the pan-sharpened image of the study area and the part used in the study are given in Figures 3.4 and 3.5, respectively. The study area extent is marked with yellow rectangle in Figure 3.4. The specs of the data used in this study are given in Table 3.3.

Table 3.2: The WV-2 satellite characteristics [63]

WorldView-2 Characteristics	
Launch Information	Date: October 8, 2009
	Launch Vehicle: Delta II 7920
	Launch Site: Vandenberg Air Force Base
Orbit	Altitude: 770 kilometers
	Type: Sun synchronous, 10:30 am descending node
	Period: 100 minutes
Sensor Bands	Panchromatic: 450 - 800 Multispectral: Coastal Blue: 400 - 450 Red: 630 – 690 Blue: 450 – 510 Red Edge: 705 - 745 Green: 510 – 580 NIR1: 760 – 895 Yellow: 585 – 625 NIR2: 860 - 1040
Sensor Resolution	0.46 meters GSD at nadir Panchromatic 1.85 meters GSD at nadir Multispectral
(GSD = Ground Sample Distance)	0.52 meters GSD at 20° off-nadir Panchromatic 2.07 meters GSD at 20° off-nadir Multispectral
NIIRS Equivalency	NIIRS potential of greater than 5.0
Dynamic Range	11-bits per pixel
Swath Width	16.4 kilometers at nadir
Pointing Accuracy & Knowledge	Accuracy: <500 meters at image start and stop
	Knowledge: Supports geolocation accuracy below
Retargeting Agility	Acceleration: 1.43 deg/s/s
	Rate: 3.86 deg/s
	Time to slew 200 kilometers: 10 seconds
Onboard Storage	2199 gigabits solid state with EDAC
Max Viewing Angle / Accessible Ground Swath	Nominally +/-45° off-nadir = 1651 km wide swath Higher angles selectively available
Per Orbit Collection	524 gigabits
Max Contiguous Area Collected in a Single Pass	138 x 112 km mono 63 x 112 km stereo
Revisit Frequency to target at 40° N latitude	1.1 days at 1 meter GSD 3.7 days at 20° off-nadir or less (0.52 GSD)
Geolocation Accuracy (CE90)	Specification of 5 m CE90 at less than 30° off-nadir, with predicted performance in the range of 4.6 to 10.7 meters (15 to 35 feet) CE90, excluding terrain and off-nadir effects With registration to GCPs in image: 2.0 m (6.6 feet)

Table 3.3: WV-2 Data Bundle used in the study

Data Name	Bands	Spatial Resolution	Radiometric resolution	Acquisition Time	Cloud Cover	Processing Level
Multi Spectral	RGB + NIR	2 meters	11 bits	07-May-15 9:02:27	0.00	Standard2A
PAN	Pan	0.5 meters	11 bits	07-May-15 9:02:27	0.00	Standard2A
Pan Sharpened	RGB	0.5 meters	11 bits	07-May-15 9:02:27	0.00	Standard2A

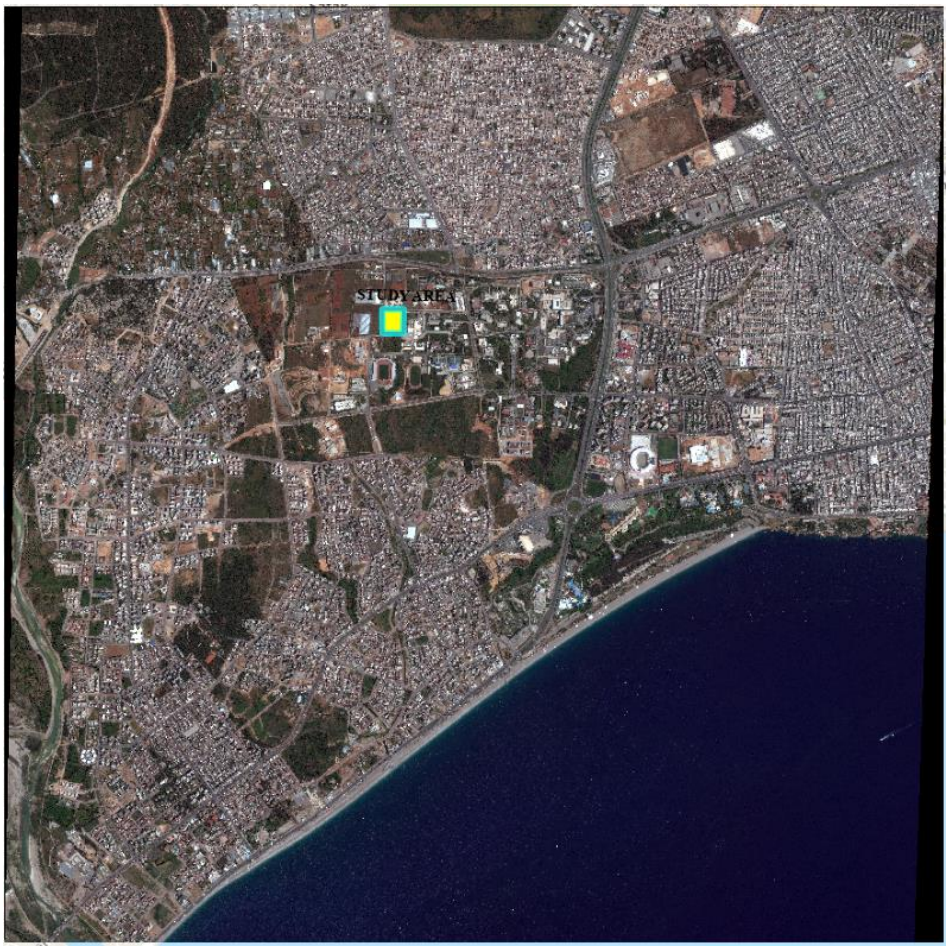

Figure 3.4: An overview of the WV-2 MS image used in the study.

Figure 3.5: Pan Sharpened WV-2 MS image (left) part and the manually delineated ground-truth map (right) over the study area

3.3 UAV Data Characteristics

A rotary-winged multi-copter system (Figure 3.6) was used to obtain the VHR images used in the study. The complete system weighed around 2.75 kgs with an extra payload including a ZeroTech flight control system and GoPro HERO3+ Black Edition camera. The camera was calibrated using the Agisoft Lens software package to calculate interior orientation parameters (Table 3.4), since the camera is not mainly built for photogrammetric purposes [64] and is not metric. The image bundle consists of a total of 125 RGB images with an overlap rate of 60%-90% and with an average footprint of 1.6 centimeters. The images were captured on 10 January 2015. The orthophoto of the study area with 2 cm spatial resolution is shown in Figure 3.7.

Figure 3.6: The Rotary-Winged Multi-Copter UAV and Camera

Table 3.4: Camera Interior Orientation Parameters [64]

Variable	Parameters (pixel)
f (focal distance)	1.6792915746501974e+003
Cx (principal point coordinate in x)	1.5071944256835432e+003
Cy (principal point coordinate in y)	1.1241168025668355e+003
k1 (radial distortion coefficient)	-2.3975802980138777e-001
k2 (radial distortion coefficient)	8.5264077044722220e-002
k3 (radial distortion coefficient)	-1.7834637858183136e-002

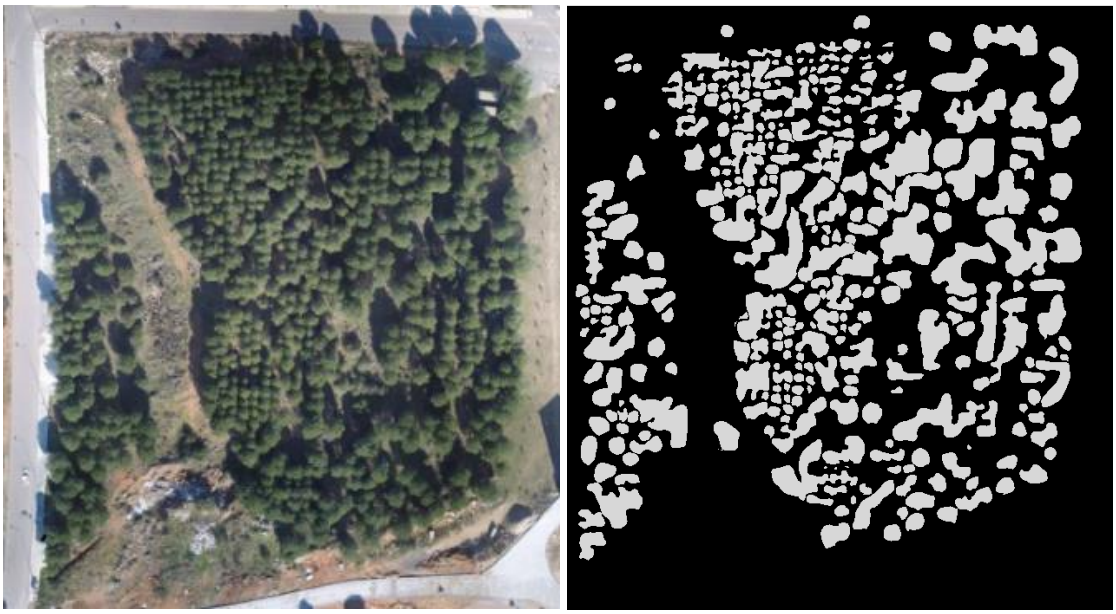

Figure 3.7: UAV Orthophoto (left) and the manually delineated ground-truth map (right) of Study Area

3.4 GK-1 Sensor & Data Characteristics

Göktürk-1 is an optical EO satellite (Figure 3.8) launched by the Turkish Ministry of Defense on 5 December 2016 in collaboration with VEGA (Italian: Vettore Europeo di Generazione Avanzata) rocket from Europe's Space Centre in Kourou, French Guyana [65]. The satellite operates with the push-broom principle and obtains high-resolution images in both pan and MS bands with 0.5 m and 2 m ground sampling distances (GSDs), respectively. The satellite moves on a Sun Synchronous Orbit (SSO) with an altitude of approximately 700 km. The lifetime of the satellite is expected to be around seven years. The VHR camera obtains images in five spectral bands, such as Panchromatic, Red, Green, Blue and NIR (Near Infra-Red) [66].

Operation responsibility of Göktürk-1 belongs to the Turkish Air Force (TURAF) Command at the location of Göktürk Ground Station (GGS). GGS is also responsible of processing the data and generating L2A data by IPS (Ingestion and Processing Services) [67]. Göktürk-1 is designed to provide high-resolution data for a wide range of applications such as military and civilian applications [65].

Figure 3.8: GK-1 Satellite [68]

The imagery bundle used here includes Pan image and 4 MS bands (RGB + NIR). The radiometric resolution is 12 bits and the cloud cover is 3%. Further information on the satellite and instrument specifications is given in Table 3.5. Image bundle and the overview of the study area with GK-1 pan image can be seen in Table 3.6 and Figure 3.9, respectively. In Figures 3 3.10, the image part of the GK-1 MS bands over the study area given.

Table 3.5: Full Specifications of GK-1 Satellite Sensor[68]

Launch Date	December 5th, 2016
Orbit	Sun synchronous
Altitude	Minimum 686 km
Equatorial pass local time	10:30 AM
Orbit Inclination	98,112°
Sensor type	Optical pushbroom
Spatial resolution	Panchromatic: 0.5 m Multispectral: 2 m
Spectral bands (µm)	0.45-0.84 µm (Panchromatic) 0.435-0.554 µm (Blue) 0.493-0.607 µm (Green) 0.606-0.717 µm (Red) 0.691-0.933 µm (NIR)
Detectors	Panchomatic 31600 pixels Multispectral 7900 pixels
PAN MTF Nyquist	Measured 0.22
PAN SNR	147 @ TDI 20
NIIRS Class	6
Radiometric resolution	12 bits
Repeat Cycle	21 days (307 orbits)
Roll / Pitch Angle	± 45° / ±30°
Swath width	15 km (Nadir)
Images on board storage	1 Tbits (278 spot CR 1:4)
Image Capacity	902 spot images (acquired and download per day)
Max. Stereo Strip Length	410 km length in single pass

Table 3.6: GK-1 Data Bundle characteristics used in the study.

Band / Product	Bands	GSD	Bit Depth	Acquisition Date & Time	Cloud Cover	Processing Level
Multi Spectral	RGB + NIR	2.5 m	12 Bits	12 September 2019 07:50:02	%3	Level 2A
Pan	Pan	1 m			%3	Level 2A
Pan Sharpened	RGB	1 m			%3	Level 2A

Figure 3.9: GK-1 pan band image used in the study.

Figure 3.10: GK-1 MS image (left) and the manually delineated ground-truth map (right) part in the study area.

4. METHODOLOGY

4.1 Workflow

The methodology preferred here is based on extraction prominent features and vegetation indices from the images and vegetation mapping based on classification of each image based on a supervised classification technique (i.e. Random Forest). However, several feature extraction and thresholding methods have also been evaluated for analyzing the potential of such methods with the input datasets, which were explained in the previous Chapter. The general workflow (Figure 4.1) of this study consists of the following five stages:

1. Preparation of input data
2. Radiometric and geometric pre-processing
3. Feature extraction and vegetation mapping
4. Change detection
5. Quality assessment

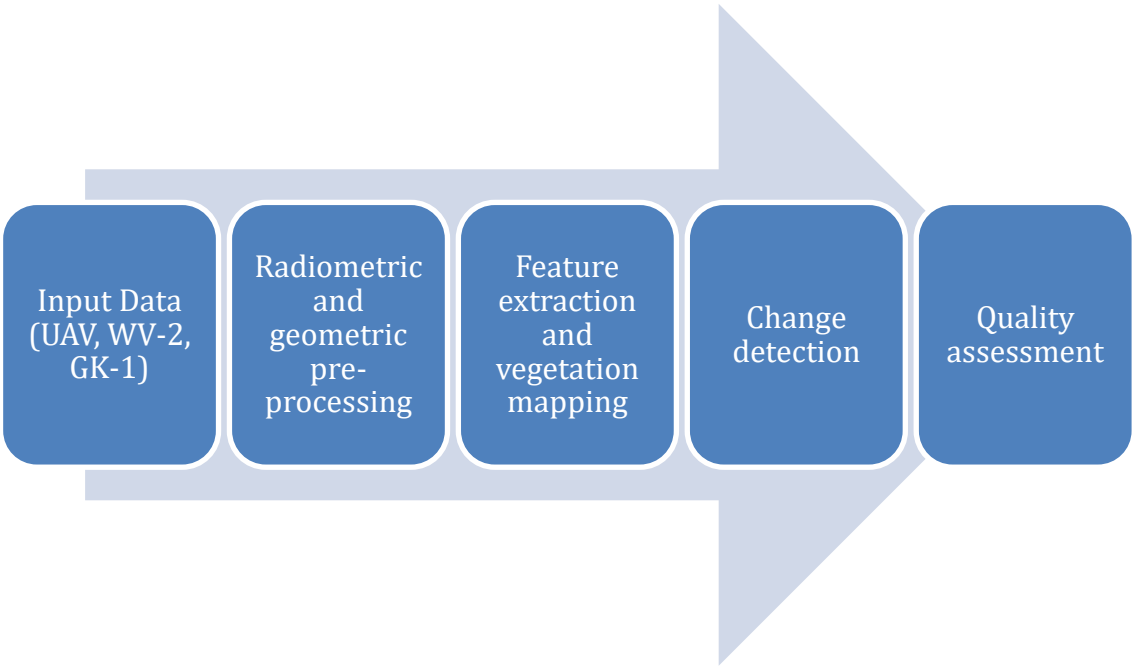

Figure 4.1: Overall methodological workflow.

Steps 4-5 are explained in the following sub-sections in detail.

4.2 Data Pre-Processing

In data pre-processing, the data were prepared for the vegetation mapping analyses to increase their performance. These preparation steps can be categorized as reduction to 8 bits and geometric processing; and include georeferencing of UAV and GK-1 datasets for accurate alignment; processing of UAV images for orthophoto and DSM generation, clipping the input datasets for the selected study region in order to investigate various feature / texture extraction methods efficiently. Each dataset was reduced to 8 bits in terms of radiometric resolution. The data pre-processing steps are depicted schematically in Figure 4.2.

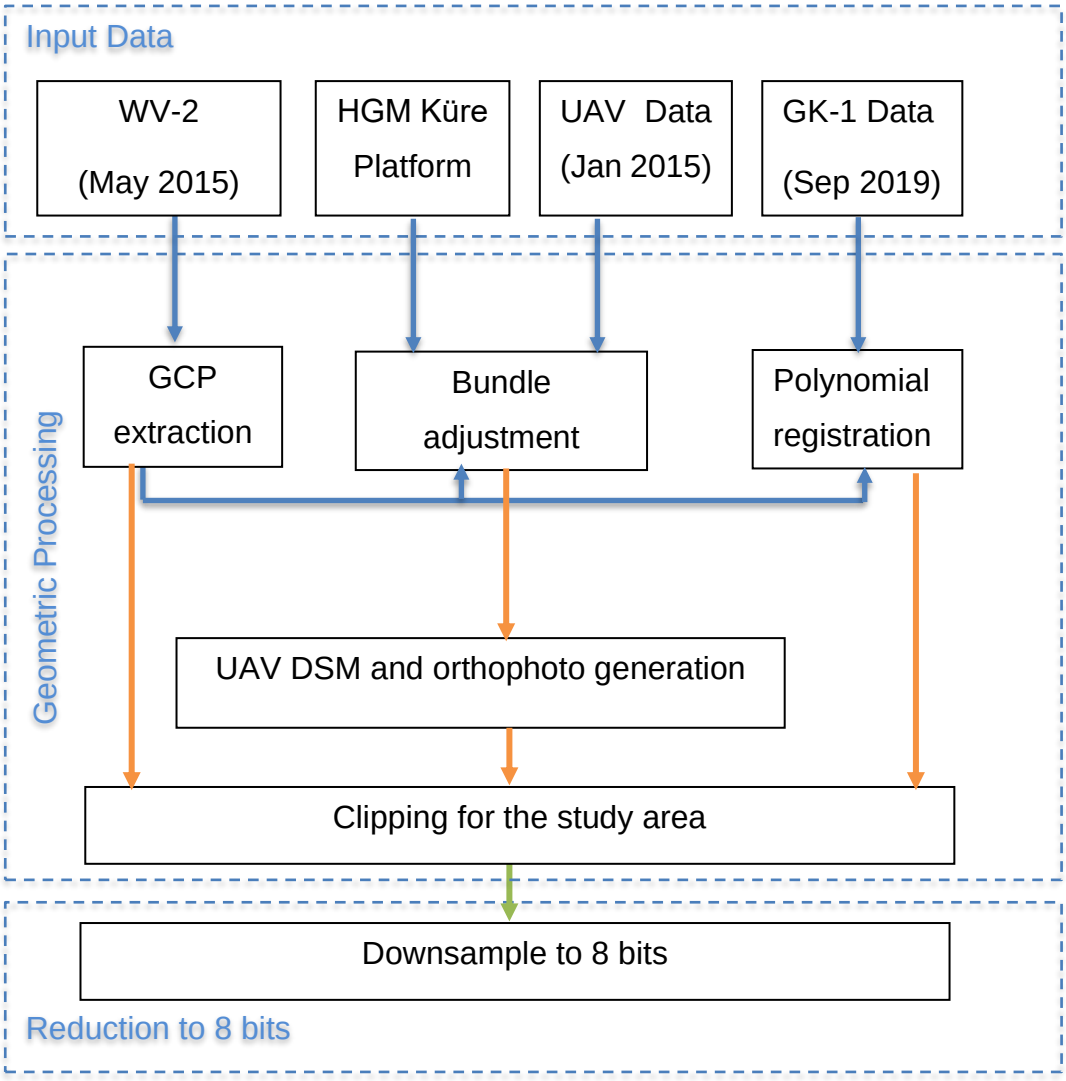

Figure 4.2: Data pre-processing methodology.

For the georeferencing tasks, the WV-2 image was taken as reference in planimetry for both the UAV and the GK-1 data. The elevation information required for the bundle block adjustment of UAV images was obtained from the web-supported desktop geographical information system (GIS) application (HGM Küre Platform) [69] of General Directorate of Mapping, Turkey. The platform provides very high resolution digital orthophotos and DEMs of Turkey. The planimetric coordinates of the ground control points (GCPs) used for georeferencing of UAV data were derived from the WV-2 images whereas the elevations were obtained from the HGM Küre. The selection of GCPs (a total of 12 points) were carried out on WV-2 due to the visibility requirement of the points on both images, which was relatively difficult due to the temporal differences in data acquisition and the resolution differences. The points were mainly selected on man-made objects in an extended study area (Figure 4.3). After the georeferencing, the UAV orthomosaic and the DSM was produced. The DSM was not employed in further processing since the compared datasets involved 2D information only. The UAV images were processed by using Agisoft Metashape Pro 1.7.1 software [70]. The bundle adjustment, DSM and orthophotos generation steps are explained in detail in Agisoft Orthophoto Tutorial [71]. The UAV data processing workflow is presented schematically in Figure 4.4.

Figure 4.3: UAV orthorectification with GCPs

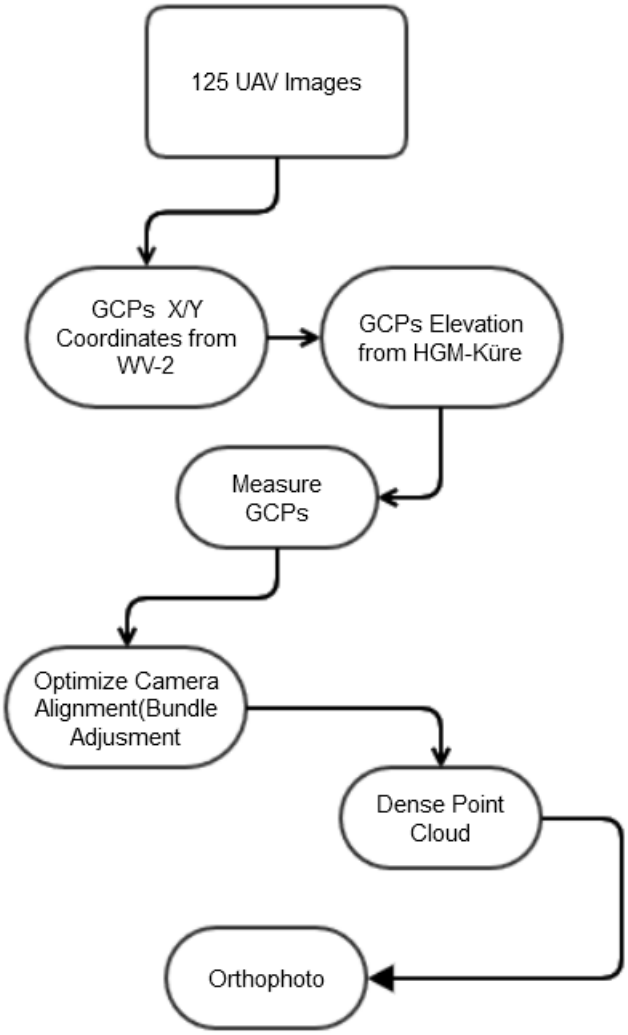

Figure 4.4: UAV data processing procedure.

The WV-2 and GK-1 were co-registered using a polynomial method by using the planimetric coordinates of the GCPs. A 2nd order of polynomial function was applied for the task. A total of 9 points was identified in both images. The GCP selection, coordinate information extraction, and the polynomial registration were carried out manually using ArcMap 10.8 [72].

In terms of radiometric processing, the tasks performed were relatively simple. The satellite images used in this study are radiometrically corrected and did not need further processing other than reducing them to 8 bits for further analysis which was performed using ArcMap 10.8 Export Raster tool [72]. Besides the satellite images, UAV orthophoto

and vegetation index results were reduced to 8 bits for further analysis. Radiometric processes were carried out using ArcMap 10.8.0 [72] export to raster tool.

4.3 Feature Extraction and Vegetation Mapping

Several image enhancement techniques, texture extraction methods and vegetation index calculations were applied to the datasets. All the tested methods are presented in Table 4.1. These methods were chosen based on the recent studies about the topic. Some of the methods were not utilized for the final vegetation mapping due to poor information extraction performance in one or more datasets.

Table 4.1: Image radiometric enhancement, texture and vegetation index extraction methods applied in the thesis.

Method	Product	UAV data	WV-2 data	GK-1 data
LBP [73]	Textural information extraction	Tested	Tested	Tested
Gaussian filter + LBP	Noise reduction and textural information extraction	Tested	Tested	Tested
GRVI	Vegetation index	Used	Used	Used
NDVI	Vegetation index	Used	Used	Used
Local Maxima	Textural information extraction	Tested	Tested	Tested
Local Minima	Textural information extraction	Tested	Tested	Tested

The RF ensemble method was used for the supervised classification of vegetation from the extracted features and vegetation index images. Furthermore, several image thresholding methods were investigated for the unsupervised mapping of the vegetation from the image products. The details are presented in the following sub-sections.

4.3.1 Vegetation Indices

A vegetation index is commonly used for the identification of vegetation in various areas. NDVI requires a near-infrared (NIR) band for computation. The NIR band data are available with GK-1 and WV-2, but not for UAV. The MS images of GK-1 and WV-2 were used to calculate NDVI as following:

$$NDVI = \frac{NIR-Red}{NIR+Red}$$

The GRVI [10] is calculated only using red and green band images. Due to the lack of NIR band in UAV image, GRVI was the most suitable option to use instead of NDVI. In order to analyze its effect on the satellite images, pan-sharpened GK-1 and WV-2 data were also processed with the same algorithm. The formulation of GRVI is as follows:

$$GRVI = \frac{Green - Red}{Green + Red}$$

Vegetation indices were included in the application of RF. Pan-sharpened images of GK-1 and WV-2 were used together with NDVI and GRVI; while UAV orthophoto was processed only with GRVI due to availability.

4.3.2 Local Maxima and Minima

The darkest pixels in an image are minima, on the other hand, maxima are the brightest pixels in terms of pixel values. Local minima and local maxima were applied to each dataset to identify the trees. Local maxima algorithm was applied to identify trees and local minima algorithm was applied to identify bare lands and shadows.

The scikit-image Python library [74] was used to implement local maxima algorithm and Mahotas Python library [75] to apply local minima. The implemented codes are given in Figure A.1 and Figure A.2 in Appendix.

4.3.3 Mapping with Random Forest

The RF is a modified decision trees (DT) ensemble learning method [77], which requires supervised training. A DT is created with the start root node of the tree and advancing down to internal nodes and the last part of leaves [78]. The method's basic principle is to select the samples from training labels and followed by training of the system with subset data set to create a prediction model [79].

The RF classifier implemented in scikit-learn [80] was applied using Python 3.9 programming environment.. The RF classifier was tested on datasets together with the NDVI and GRVI results depending on the availability.

The OpenCV library [81] for Python was used for image read-write operations. The selected classes on orthophotos were shadow areas, trees, and bare land. Only two classes were defined for the classification of GRVI and NDVI images that are vegetation and bare land. The training areas were selected manually based on these groups. For visualization and plotting, Python matplotlib 3.3.4 library was used. The sample code for classification of the UAV image is represented in Figure A.3 in Appendix. The parameters used in the RF algorithm as follows;

- n_estimators defines the number of trees in the forest
- intensity is the image intensity
- edges is the usage of Canny Edge Detection
- texture is the image's textural appearance
- sigma_min minimum radius of the isotropic filters used to create the features
- sigma_max maximum radius of the isotropic filters used to create the features
- n_jobs is the number of jobs that run accordingly
- max_depth defines the maximum depth of the tree, the nodes will be expanded until a specified number
- max_samples If bootstrap is True, the number of samples to draw from X to train each base estimator.

In image classification, accuracy analysis is essential. To compute the accuracy, training areas and test areas were given as input into RF algorithm and split the data with a ratio of 80/20. A confusion matrix was created in order to calculate the overall classification accuracy. In scikit learn library [82] there is an option to print out the classification report where accuracy rate is available. Also, manually delineated ground-truth maps were compared using pixel-based methods for accuracy evaluation. Other than using statistical methods, a visual interpretation approach was employed as well. The resulting images were compared with the original images to ensure the quality of the results. ArcGIS Pro 2.8 [72] was used to compare the results with the original images. ArcGIS Pro Swipe tool was used for the visual assessment.

The F1-score is the measure of a machine learning model's accuracy on a dataset. It's been used widely to estimate binary classification problems which classify data into positive and negative. Formula for the F1-score is given in the equation below [83].

$$F_1 = \frac{2}{\frac{1}{\text{recall}} \times \frac{1}{\text{precision}}} = 2 \times \frac{\text{precision} \times \text{recall}}{\text{precision} + \text{recall}}$$
$$= \frac{\text{tp}}{\text{tp} + \frac{1}{2}(\text{fp} + \text{fn})}$$

Precision can be considered of as a measure of the accuracy of a classifier. A low precision can also indicate a large number of False Positives. Recall can be considered of as a measure of a classifiers completeness. A low recall indicates many False Negatives. The F1 score conveys the balance between the precision and the recall. True positive (tp) is the number of true positives classified by the model. True negative (tn) False negative (fp) is the number of false negatives classified by the model. False positive (fp) is the number of false positives classified by the model. The terms and classes used in this study as following;

- 0 is non-vegetation
- 1 is vegetation
- True Negative (0→0)
- True Positive (1→1)
- False Positive (0→1)
- False Negative (1→0)

4.3.4 Mapping with Image Thresholding

Vegetation mapping was done using the thresholding method on GRVI and NDVI images. For thresholding purposes, many methods were tested including the scikit-image library algorithms such as; ISODATA, mean, otsu, yen and local thresholding [73] (Figure A.4 in Appendix). Thresholding was applied to local maxima and local minima results of the image. Also, in QGIS [84], the histograms (Figure 4.5) of the images were visually inspected for the selection of threshold parameters, which were investigated to find out the optimum range to detect trees in the images. Accuracy assessment of the results were performed using a manually delineated ground-truth maps as reference and by comparing the images pixel-wise.

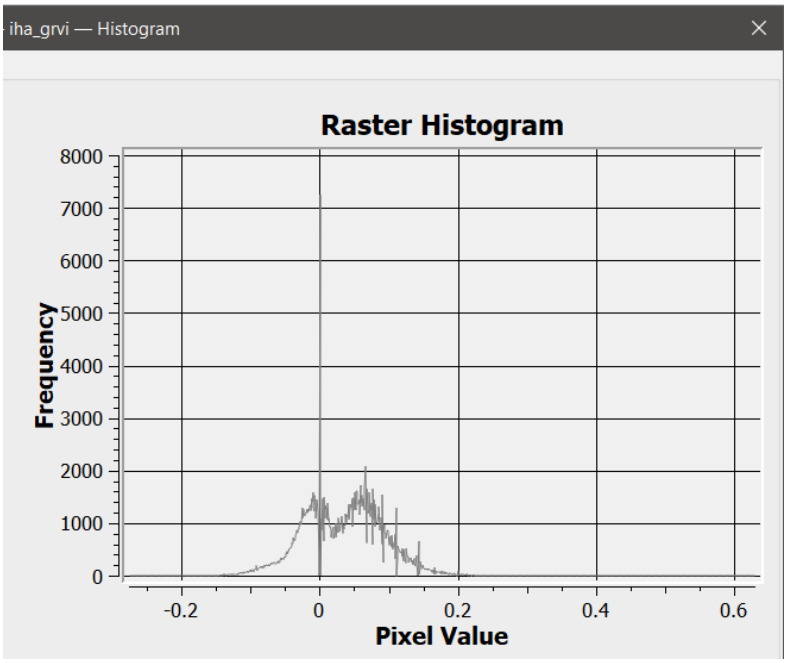

Figure 4.5: Histogram of UAV GRVI Image displayed in QGIS

Otsu thresholding algorithm will be used to detect changes in the images. For validation the thresholding results were compared with the ground-truth maps of each dataset to ensure high accuracy. For this validation purposes, F-score has been used to evaluate the thresholding results.

4.4 Change Detection Method

In forest areas, the important changes defined by FAO [85] (Food and Agriculture Organization) as deforestation, canopy cover, logging and the transformation of forest areas into agriculture, pasture, water reservoirs and urban areas. The study area analyzed in this study has been preserved by the university.

Considering the datasets have different temporal properties (i.e. GK-1 images were obtained on 12 September 2019, WV-2 images on 7 May 2015 and UAV images on 10 January 2015), the amount of expected change is higher between GK-1 images and the other two. For the change detection, the GRVI results of UAV, WV-2 and GK-1 images were compared quantitatively and also compared visually. The decision of the most successful vegetation maps from each sensor was based on the visual assessment of the

results. The selected maps to be employed in the CD process were achieved by using Otsu thresholding algorithm [86]. The images were stored as binary images, where value 1 represents vegetation and value 0 represent non-vegetation. The image pairs for comparison were selected in their chronological order based on the date of the acquisition and evaluated pixel-wise using Python. The CD images are composed of a total of four classes as following:

- Unchanged non-vegetation (0→0)
- Unchanged vegetation (1→1)
- New vegetation (0→1)
- Loss of vegetation (deforested) (1→0)

5. RESULTS

5.1 Geometric Processing Results

A major work regarding the geometric processing was to create an orthophoto from the UAV images. 125 images were used and the locations of the cameras are shown in Figure 5.1 with other relative information such as tie points, overlap and camera specifications. Camera calibration parameters and the correlation coefficients are shown in Table 5.1. A total of 81,344 tie points were produced for the bundle adjustment and the RMSE reprojection error 1.46 pixels. 12 GCPs were used for the processing. The overall processing time was 30 minutes. The spatial resolution of the orthomosaic is 2 centimeters.

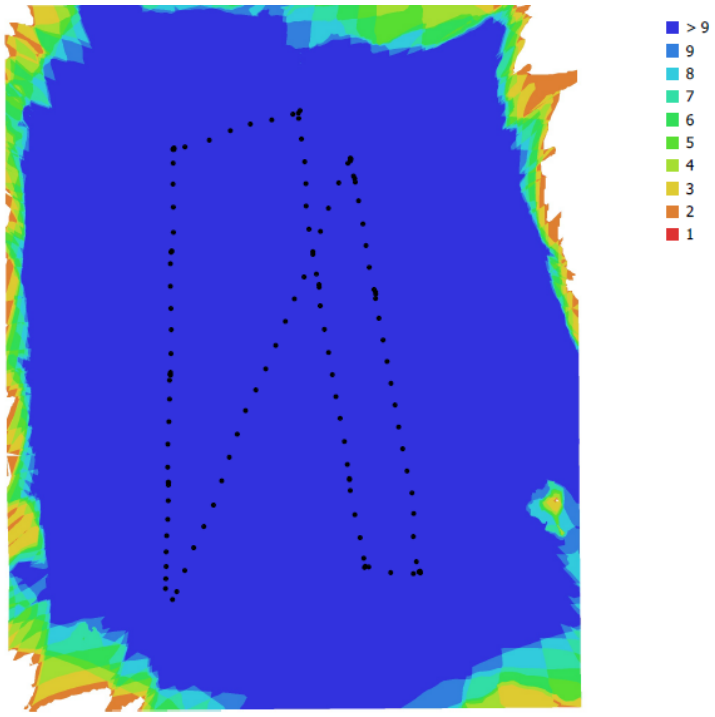

Fig. 1. Camera locations and image overlap.

Number of images:	125	Camera stations:	125
		Tie points:	81,344
		Projections:	470,995
		Reprojection error:	1.46 pix

Camera Model	Resolution	Focal Length	Pixel Size	Precalibrated
HERO3+ Black Edition (2.77mm)	3000 x 2250	2.77 mm	1.6 x 1.6 µm	No

Figure 5.1: Image perspective center locations and the camera parameters.

5.2 Radiometric Scaling

The reduction to 8 bits was carried out by downsampling the datasets for further analysis. The processing task was performed by using ArcMap. The input and output image histogram of WV-2 Pan image obtained after reduction from 11 bits to 8 bits is shown in Figure 5.2. The pixel value distribution is distributed better in 8 bits image. All datasets including the vegetation index results were scaled to 8 bits data similarly.

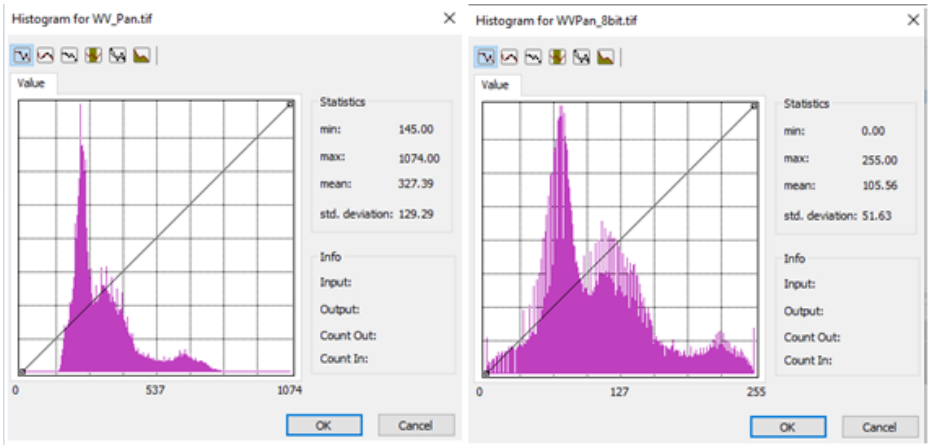

Figure 5.2: Histograms of WV-2 Pan Image in 11 bits (left) and after the reduction to 8 bits (right)

5.3 Feature / Texture Extraction Results

The GRVI and NDVI vegetation indices were produced for identifying the vegetation better. The GRVI results of all datasets are presented in Figure 5.3. The NDVI results of the satellite images are provided in Figure 5.4. The NDVI was produced only for GK-1 and WV-2 due to the lack of NIR band in the UAV data.

When the results are compared visually, it can be said that GRVI is a powerful method for highlighting vegetation information with high resolution data. The NDVI result of GK-1 is more interpretable over GRVI. The differences in the NDVI outputs of WV-2 and GK-1 can be associated with the differences in the spatial resolution and the satellite off-nadir angle.

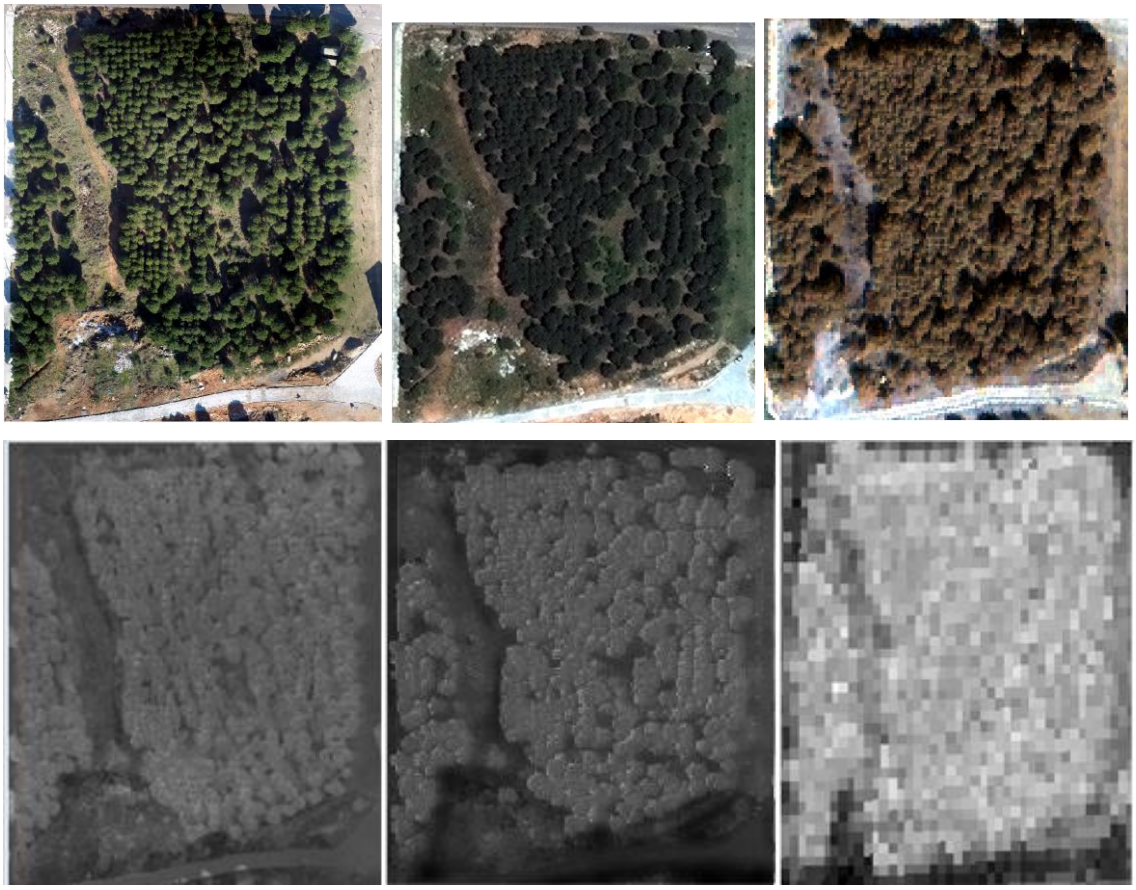

Figure 5.3: The original RGB orthophoto and pan-sharpened WV-2 and GK-1 images (above) and the GRVI results (below). Left to Right: UAV, WV-2, GK-1

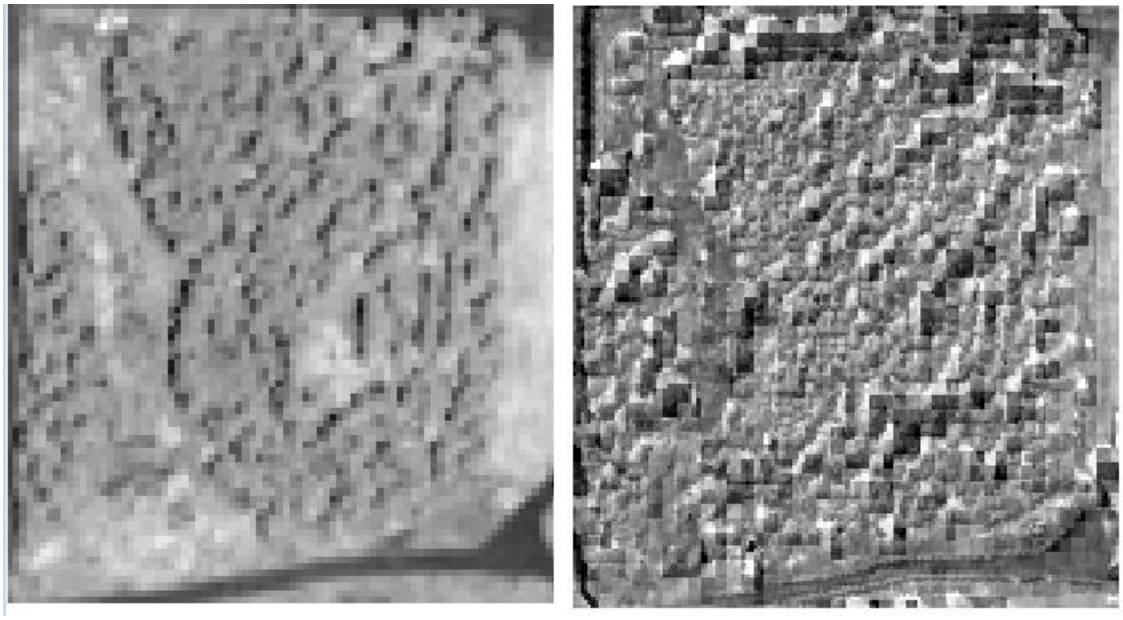

Figure 5.4: NDVI results of WV-2 (left) and right GK-1 (right).

The raw Local maxima and local minima results were not meaningful enough to use it in the methodology. These images were used for mapping with thresholding.

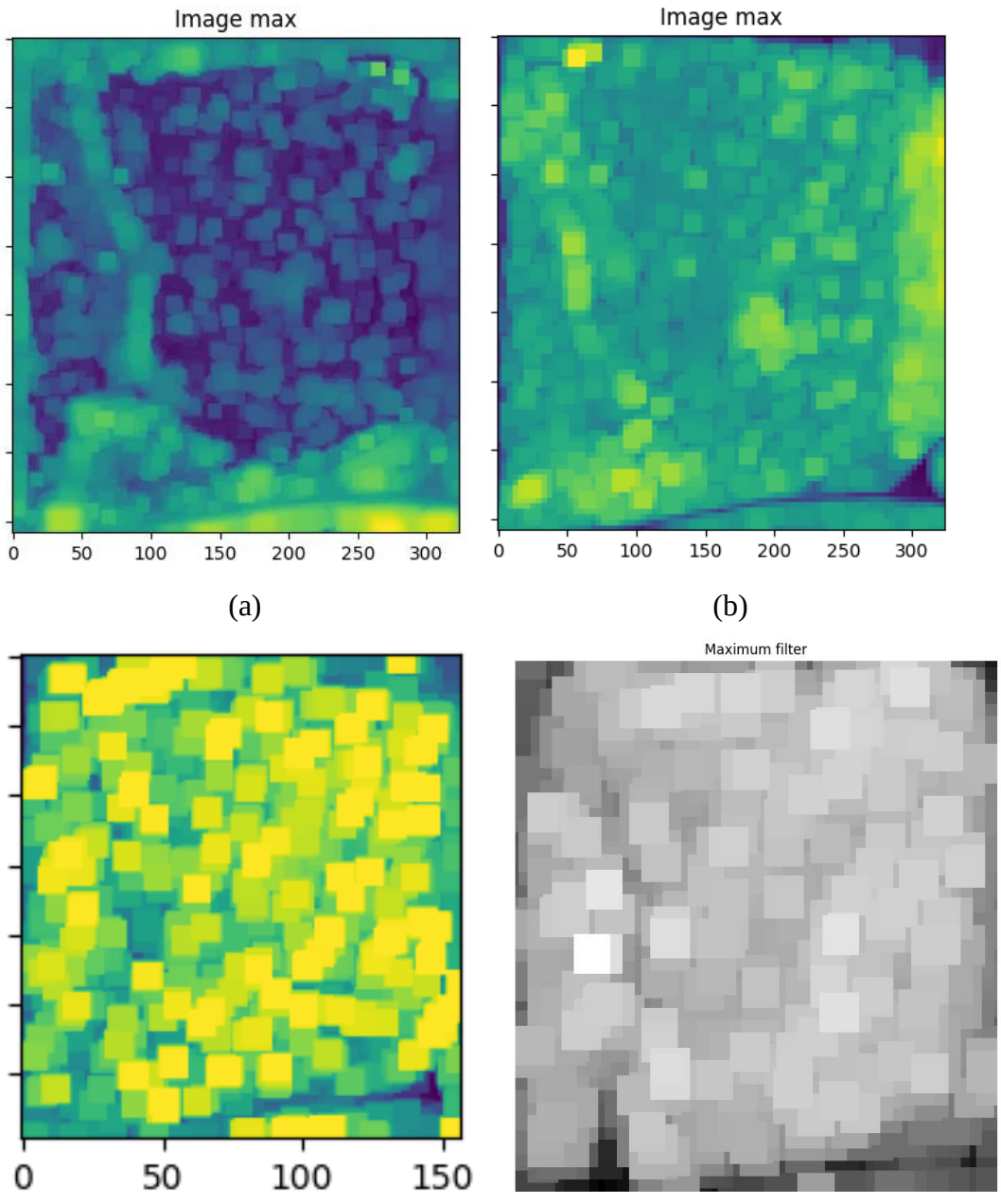

Figure 5.5: Local Maxima results: (a) WV GRVI, (b) WV NDVI, (c) GK-1 NDVI, (d) GK-1 GRVI.

5.4 RF Results

The input images and the results obtained from RF classification together with the training areas are shown in Figures 5.6 – 5.10. When the classification and segmentation results between the different sensors are compared visually (Figures 5.6-5.10), the details

in the UAV segmentation are higher thanks to the high spatial resolution. The WV-2 results are superior GK-1 results due to the same reason. When proper methodology is applied, it may be possible to count the trees in the UAV data and most trees with the WV-2 data. Only an area-based assessment would be possible with the GK-1data. Here, the UAV segmentation results can be considered as reference for the evaluation of the results obtained from the satellite imagery. The morphological similarity between the UAV & WV-2 results is higher when compared with the UAV-GK-1 results.

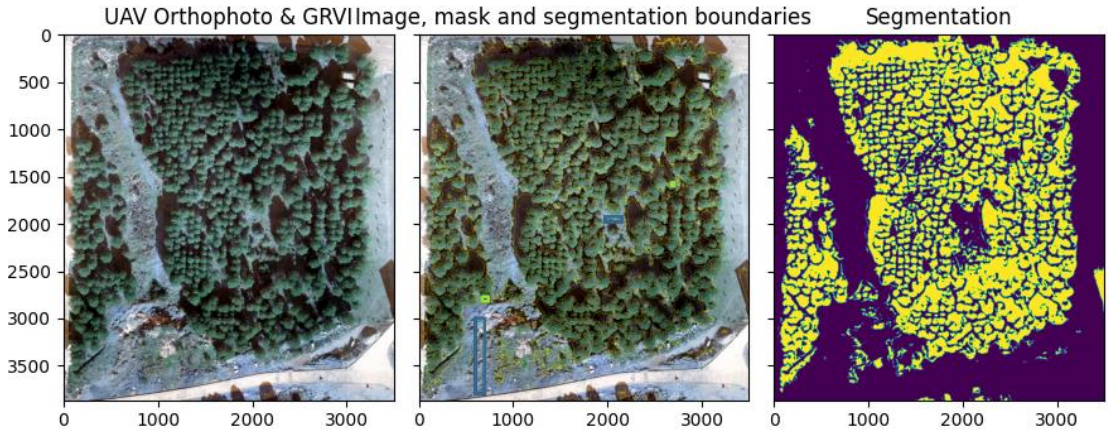

Figure 5.6: UAV Orthophoto and GRVI RF result.

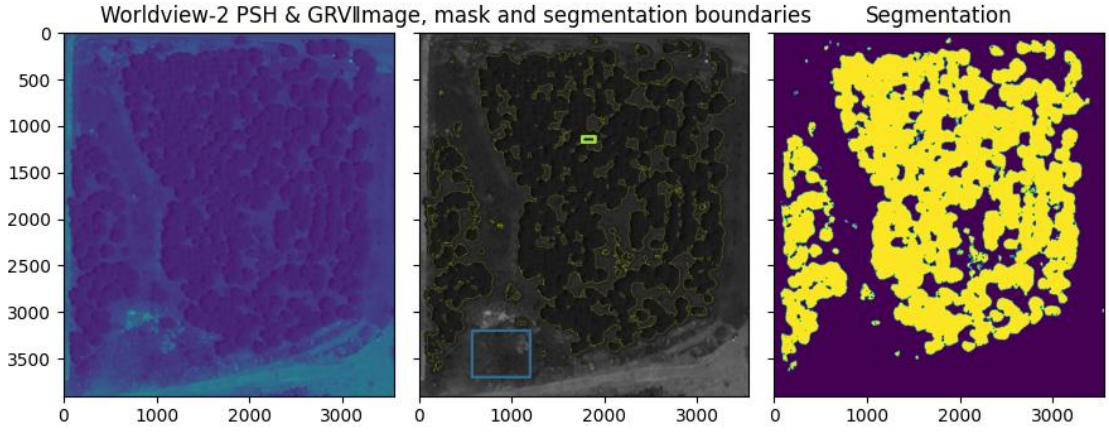

Figure 5.7: WV-2 Pan-Sharpened image and GRVI result with RF.

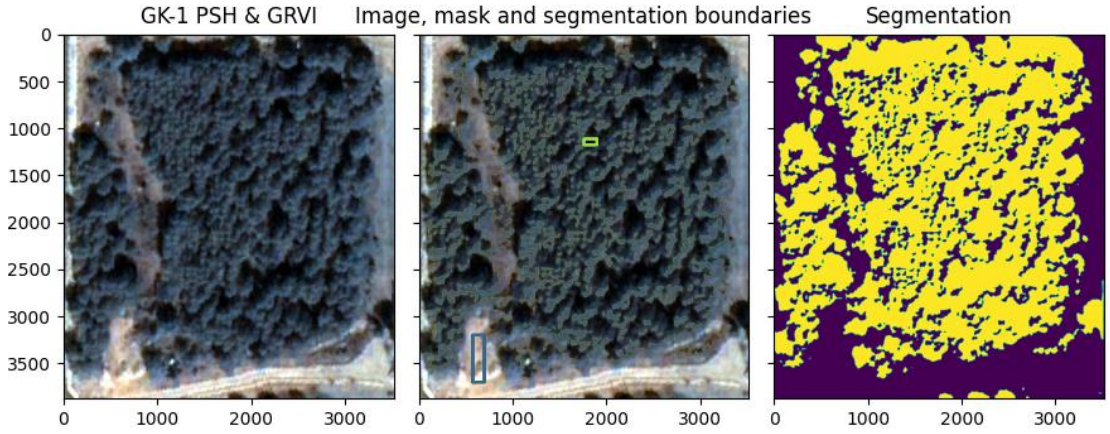

Figure 5.8: GK-1 Pan-Sharpened image and GRVI results with RF.

The RF results of WV-2 and GK-1 pan-sharpened images with NDVI presented in Figures 5.9 and 5.10 indicate that the segmentation results of the WV-2 data is in general more accurate than the GK-1 results, which can be explained with the spatial resolution difference again. The differences between GRVI and NDVI added images are not visually detectable.

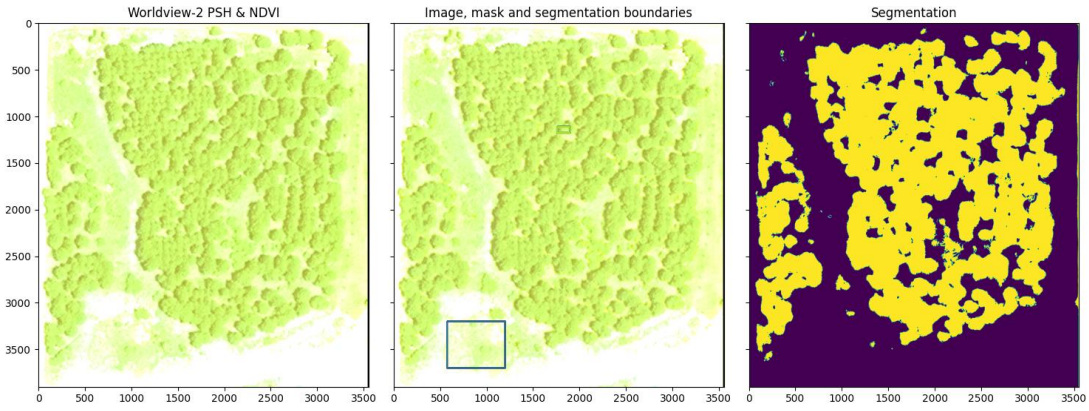

Figure 5.9: WV-2 Pan-Sharpened images and NDVI results with RF.

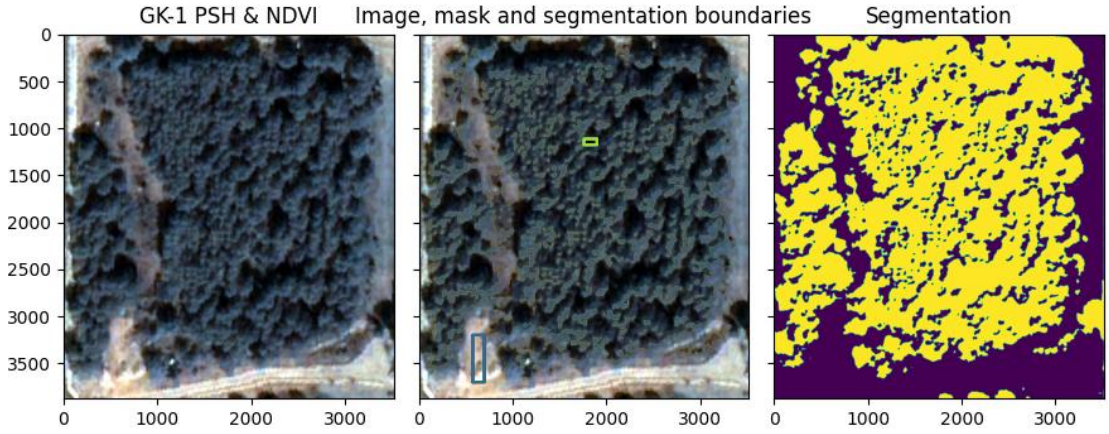

Figure 5.10: GK-1 Pan-Sharpened image and NDVI results with RF.

A major problem with the UAV data was the time of the day during the image acquisition. The images were captured before noon which caused a shadow problem. The taller trees in the area caused large shadow areas which yielded to segmentation errors. The RF result of UAV data is shown in Figure 5.11

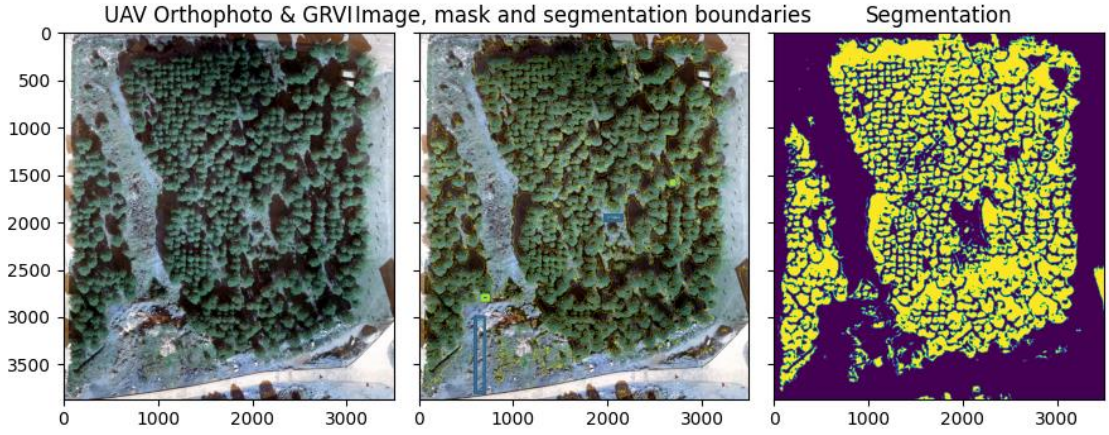

Figure 5.11: The UAV orthophoto and GRVI results with RF.

In the WV-2 GRVI and NDVI infused Pan-sharpened RF result (Figure 5.7 and 5.9), the vegetation was visible and well separated in the classification.

The RF classification with the UAV orthophoto was performed for two classes. The amount of shadow affected the classification accuracy.. Trees were mostly correct apart from the upper part of the image where shadows are dominant. The RF results with the UAV RGB data with GRVI are good enough to identify vegetation and even could be possible to distinguish individual trees. Apart from issues that originate from shadows, the classification results were successful to identify vegetation.

WV-2 pan-sharpened RF classification does not have large amount of shadows which made the classification more efficient. Bare land class was generally good other than the inclusion of the saplings in the right section of the image, and some areas between the trees were not included in the class. The vegetation class was correct in most of the image, there were no trees found in the classification. The differences between GRVI and NDVI added dataset results were not significant.

In the GK-1 GRVI and NDVI added pan-sharpened RF results, shadows caused issues in the classification and the bare land pixelswere mostly included in the right class. The major error was the little corridor between the left section and the right section of the image was included in the vegetation class.

The prediction performance results of the RF is given in Table 5.2. In general, GRVI gave better result compared to the NDVI results. The pan-sharpened and original images produced errors mostly due to the number of shadows in the images and gave poorer accuracy results than the rest of the results.

Table 5.2: RF Classification Accuracy Results

Dataset	Classes	RF Overall Classification accuracy	RF Class Accuracy
UAV Orhophoto + GRVI	2	82%	Bare Land: 82% Vegetation:85%
WV-2 Pan-Sharpened +NDVI	2	92%	Bare Land: 93% Vegetation: 90%
WV-2 Pan-Sharpened + GRVI	2	93%	Bare Land: 93 Vegetation: 90

GK-1 Pan-Sharpened + NDVI	2	88%	Bare Land: 85% Vegetation: 88%
GK-1 Pan-Sharpened + GRVI	2	93%	Bare Land: 93% Vegetation: 90%

The manually delineated ground-truth maps were compared with the RF results for all datasets. F1 score and the confusion matrices are given in Table 5.3.

Table 5.3: RF classification results obtained from ground-truth data with class confusion values and F1- scores. 0: non-vegetation. 1: vegetation

UAV RGB + GRVI	0	1	F1-scores
0	53%	16%	0,75
1	3%	28%	
GK-1 Pan-Sharpened + GRVI	0	1	
0	30%	27%	0,59
1	14%	29%	
WV-2 Pan-Sharpened + GRVI	0	1	
0	53%	14%	0,78
1	3%	30%	
GK-1 Pan-Sharpened + NDVI	0	1	
0	28%	28%	0,59
1	14%	30%	
WV-2 Pan-Sharpened + NDVI	0	1	
0	50%	16%	0,75
1	4%	30%	

5.5 Image Thresholding Results

Two thresholding techniques were employed in this study for unsupervised vegetation mapping. One method was to manually visualize the data and by testing a different range of pixel values within the image and find the optimum range for vegetation. The double threshold values used in this method are represented in Table 5.4. The threshold values were selected heuristically. GRVI results, NDVI results and the raw images of UAV and WV-2 were classified with this method. The results of GRVI and NDVI images are shown in Figures 5.12 and 5.13, respectively. The colored GRVI results are also given with colors as a better representation of vegetation areas. The UAV GRVI results were in

general good, except for the shadow areas. On the right side of UAV image, there is a shadow area that was caused by a nearby building. On the other hand, the WV-2 GRVI result was adequate to detect event the saplings. However, it was not easy to separate them from the grass. In GK-1 results, the vegetation was visible but it was difficult to evaluate the accuracy of the result due to the lower resolution and shadows.

Table 5.4: Original data range and the double threshold values of datasets.

Dataset	Original Values (Min – Max)		Threshold Values (Min – Max)	
UAV GRVI	-0.275168	0.62963	0.015	0.3
WV-2 GRVI	0.0966507	0.981651	0.3	0.9
GK-1 GRVI	-0.091453	0.327751	0.1	0.3
WV-2 NDVI	0.015398	0.680676	0.3	0.65
GK-1 NDVI	-0.500169	0.312821	-0.1	0.3

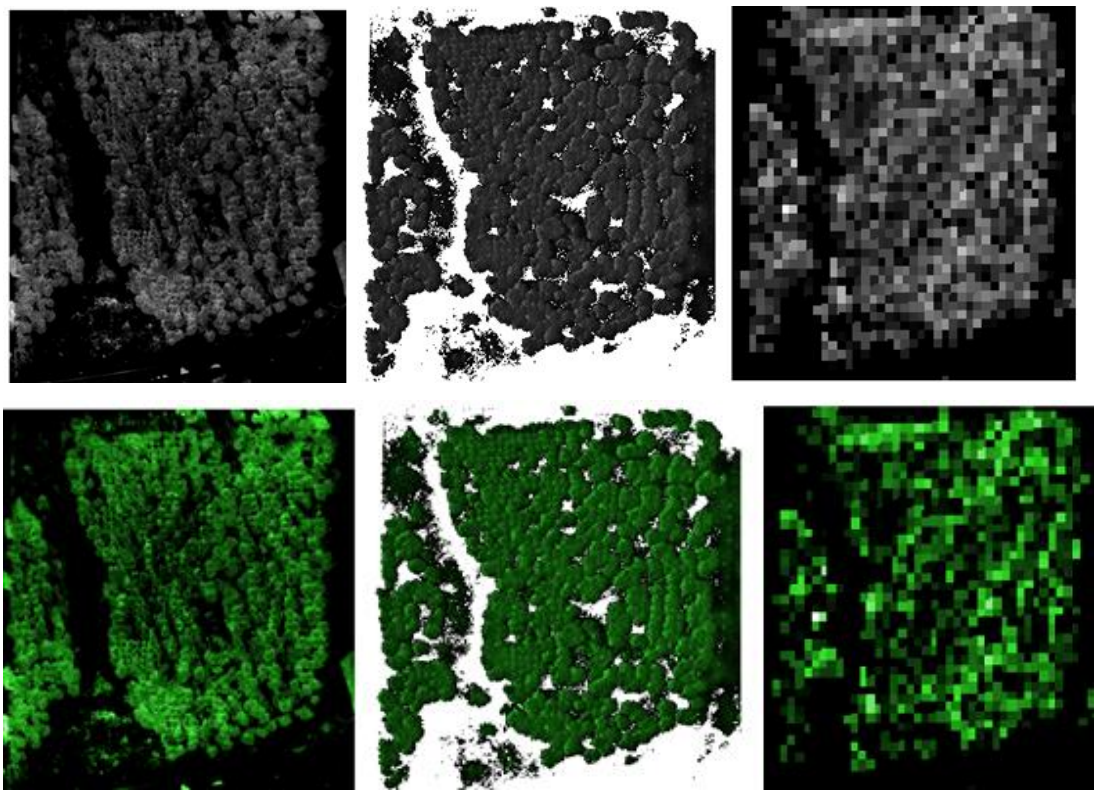

Figure 5.12: GRVI threshold binary (above) colored (below) representation results. Left: UAV, Middle: WV-2, Right: GK-1.

The NDVI threshold results from WV-2 are shown in Figure 5.13 in both binary and colored. The GRVI results were better to identify the vegetation in both satellite datasets.

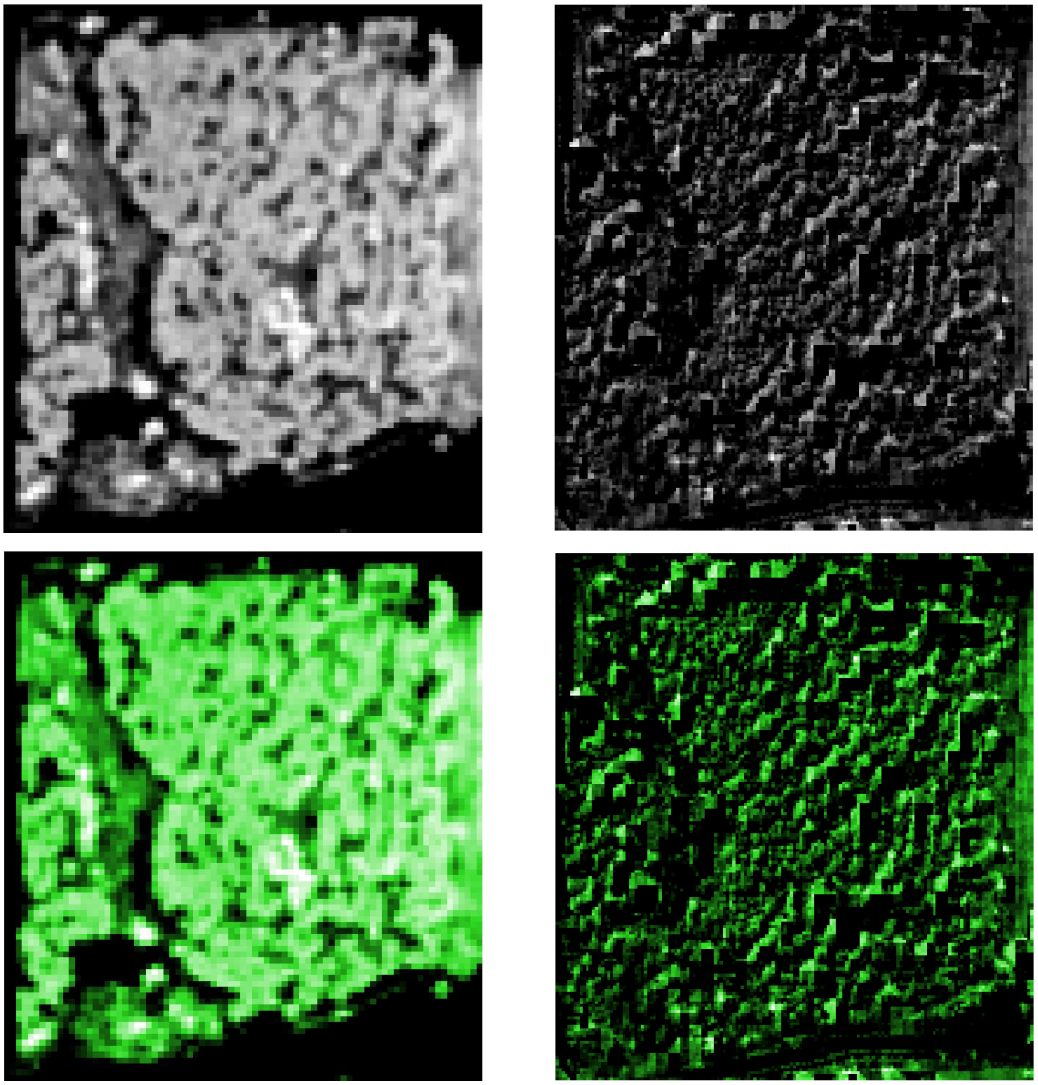

Figure 5.13: WV-2 (left) and GK-1(right) NDVI results.

Further thresholding methods were applied to datasets and their NDVI and GRVI images using the scikit-image Python library and the threshold results can be seen in Figures 5.14 - 5.22. Some of the algorithms did not create any outputs such as the *yen algorithm* in Figure 5.17. Overall, local thresholding provided better results. In most of the data isodata, mean and otsu created similar outputs despite their algorithmic differences. Overall, WV-2 GRVI (Figure 5.22) results outperformed all others visually. UAV orthophoto was good in local thresholding and the trees were easy to distinguish. Furthermore, GK-1 provided poorer results compared to the other datasets.

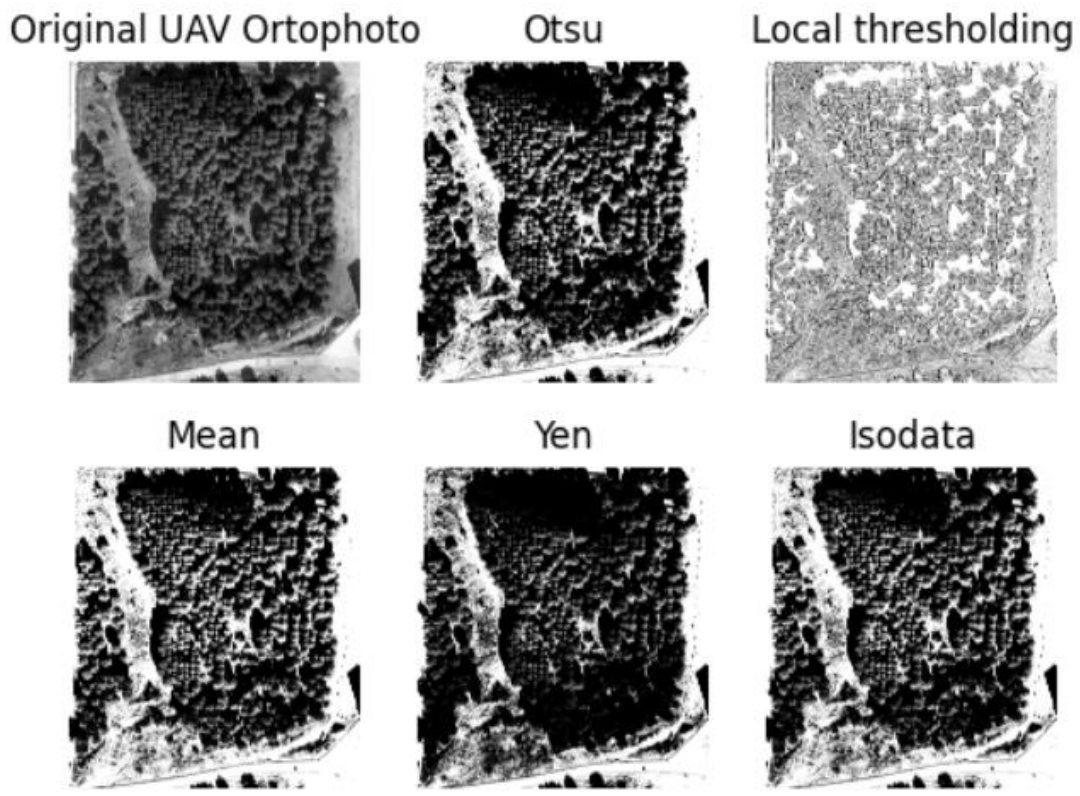

Figure 5.14: UAV orthophoto thresholding results with different methods.

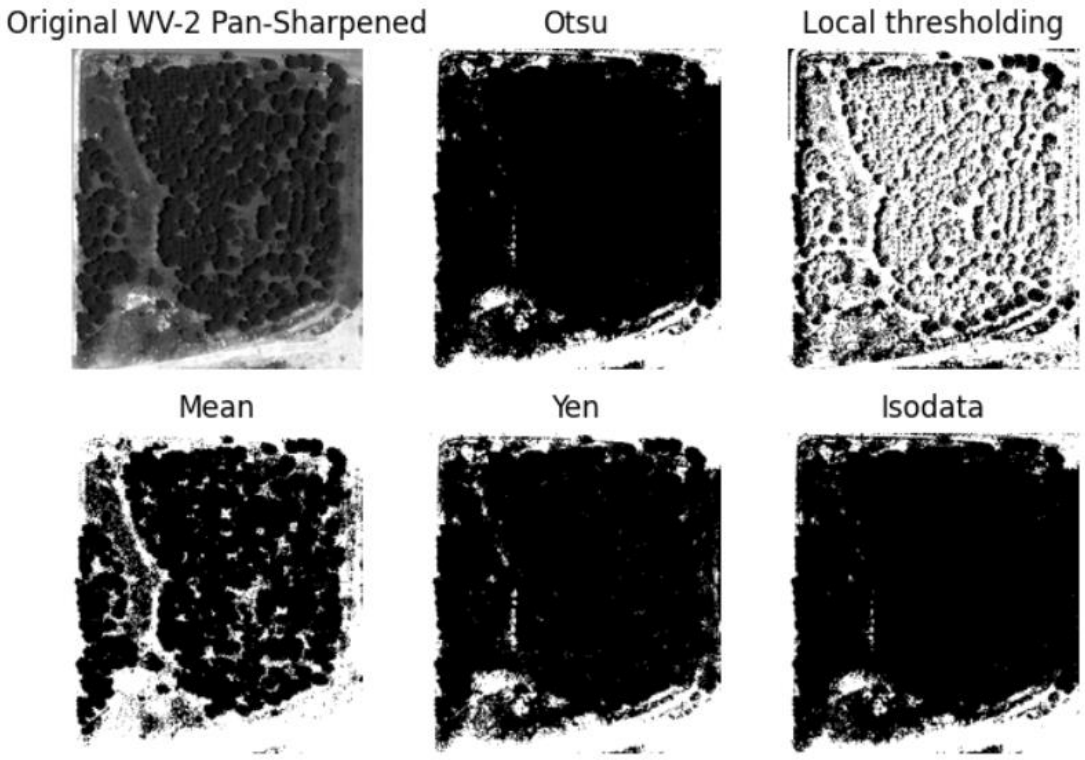

Figure 5.15: WV-2 pan-sharpened image thresholding results with different methods.

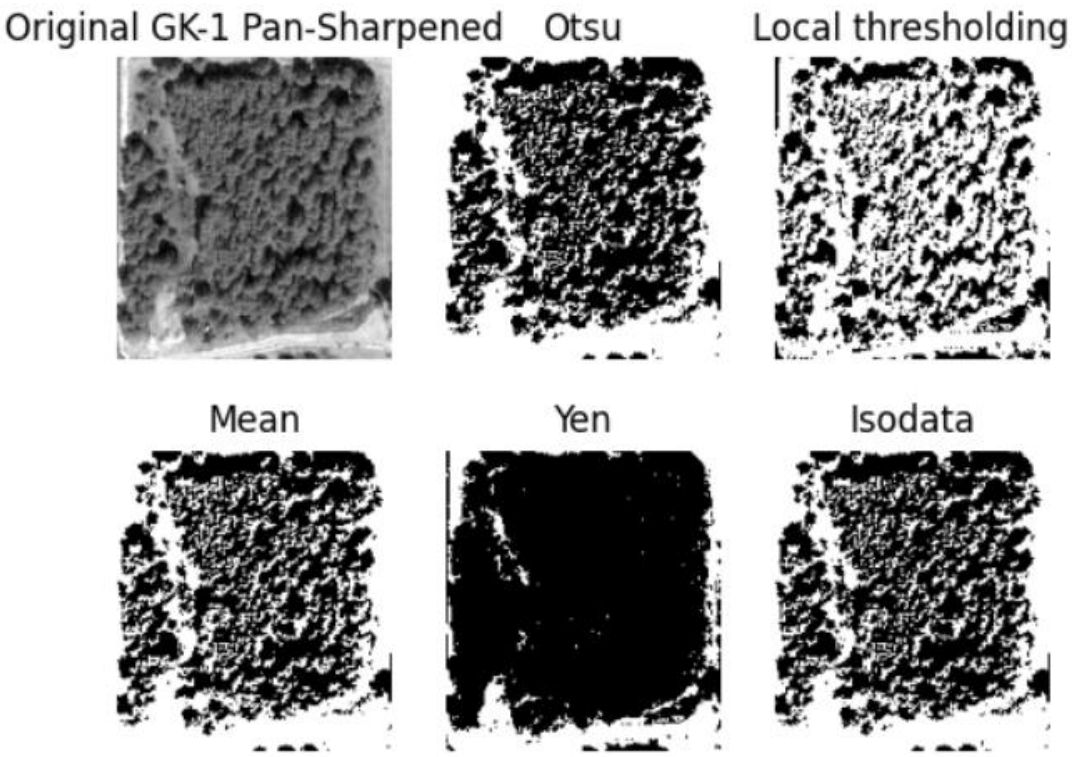

Figure 5.16: GK-1 pan-sharpened image thresholding results with different methods.

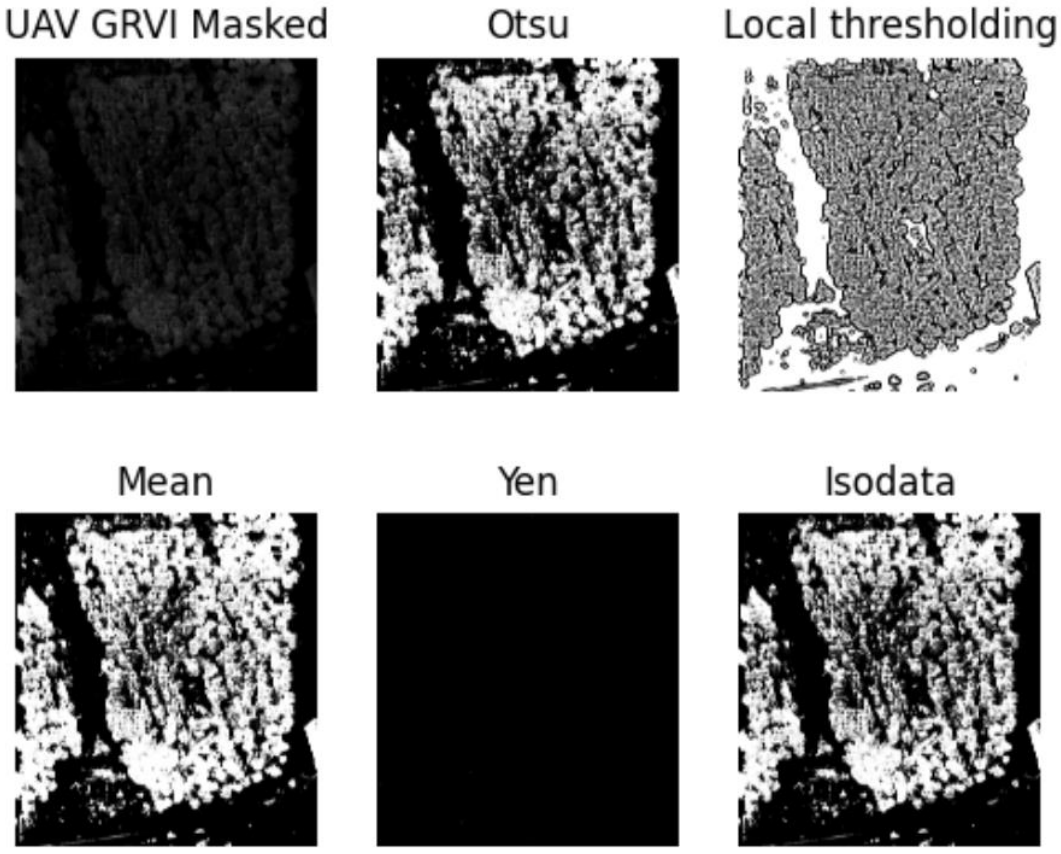

Figure 5.17: UAV GRVI Masked Threshold (masked image is shown in Figure 5.14)

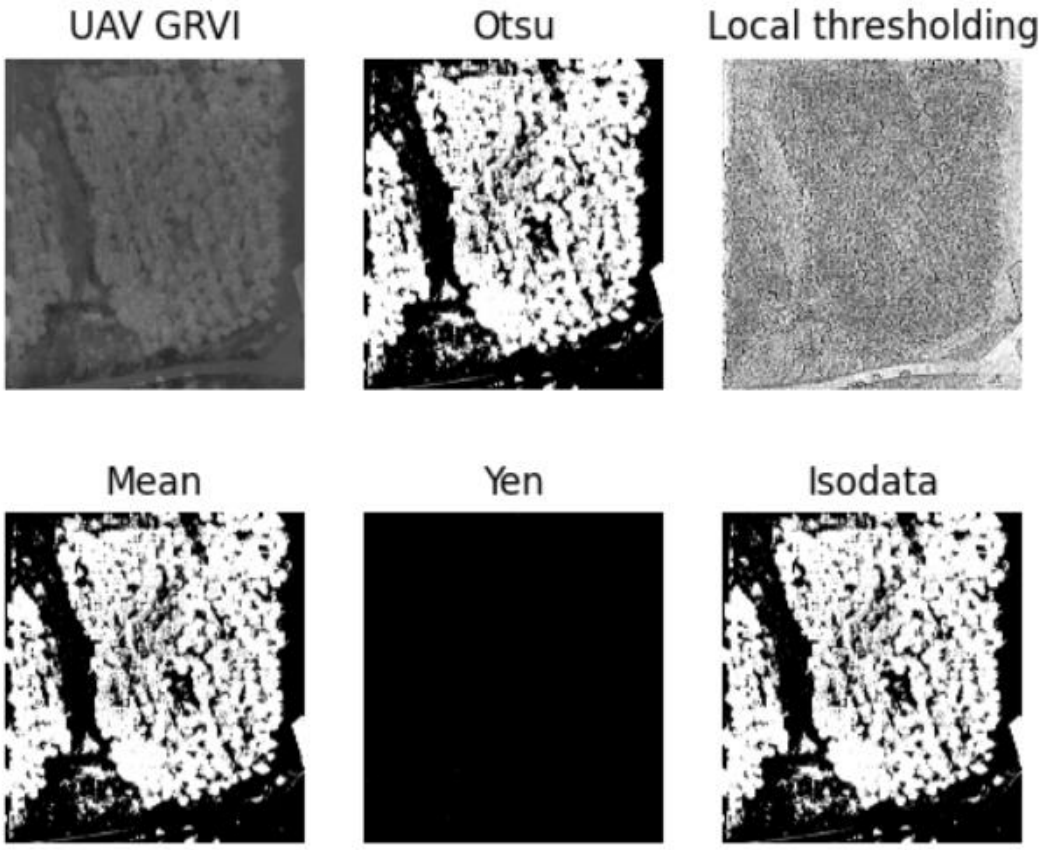

Figure 5.18: UAV GRVI Thresholds

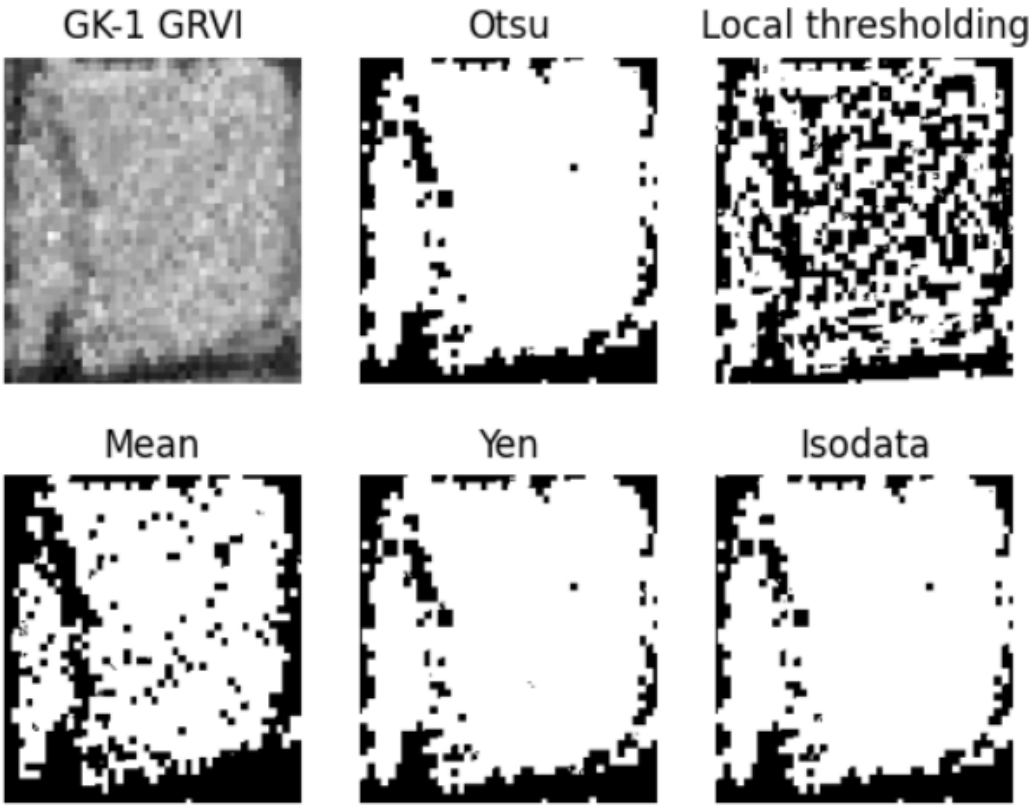

Figure 5.19: GK-1 GRVI Thresholds

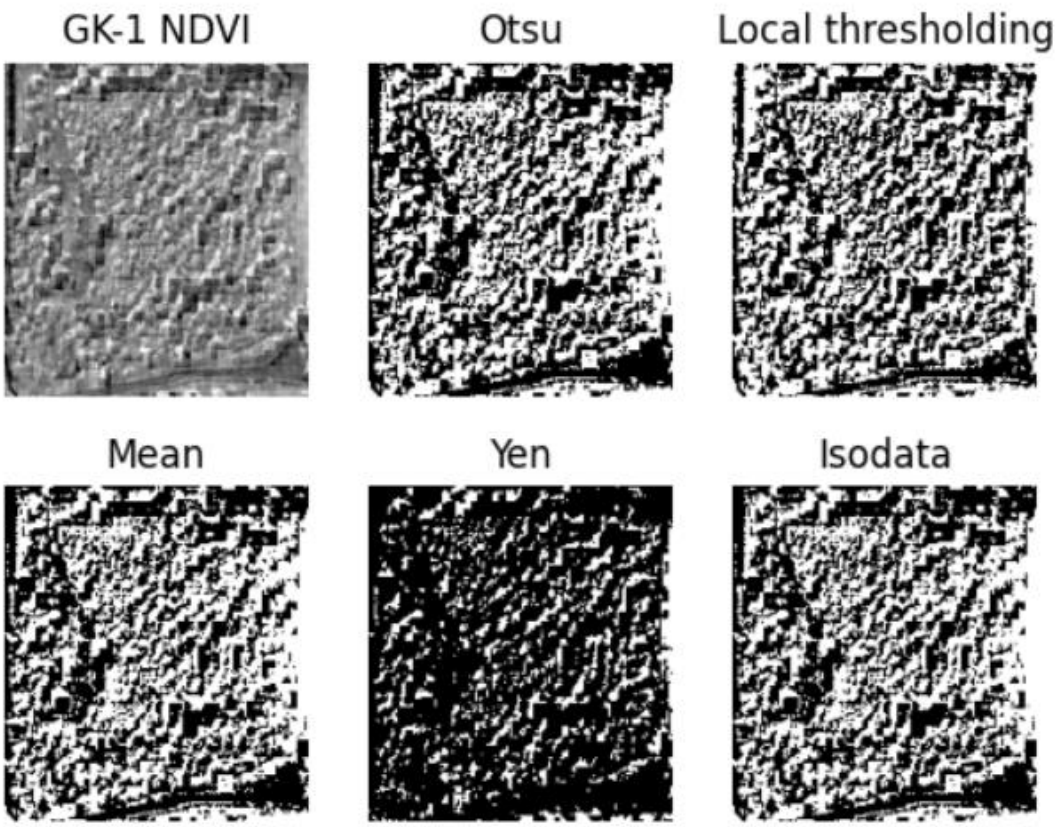

Figure 5.20: GK-1 NDVI Thresholds

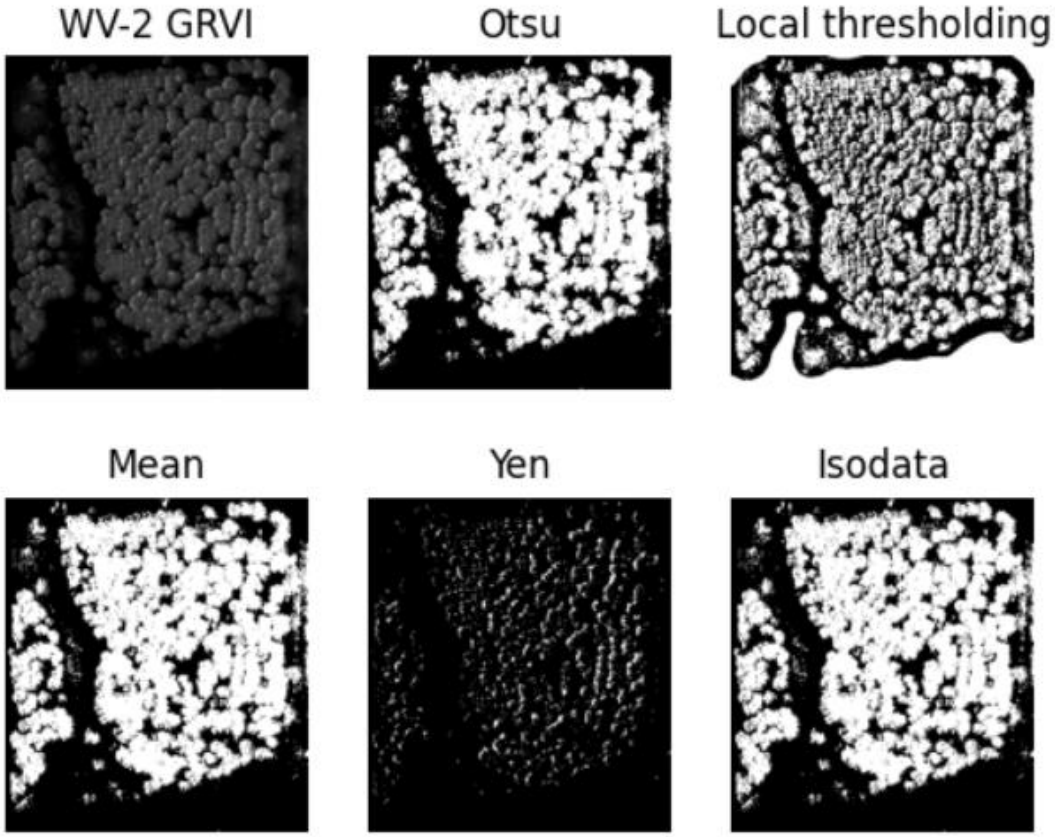

Figure 5.21: WV-2 GRVI Thresholds

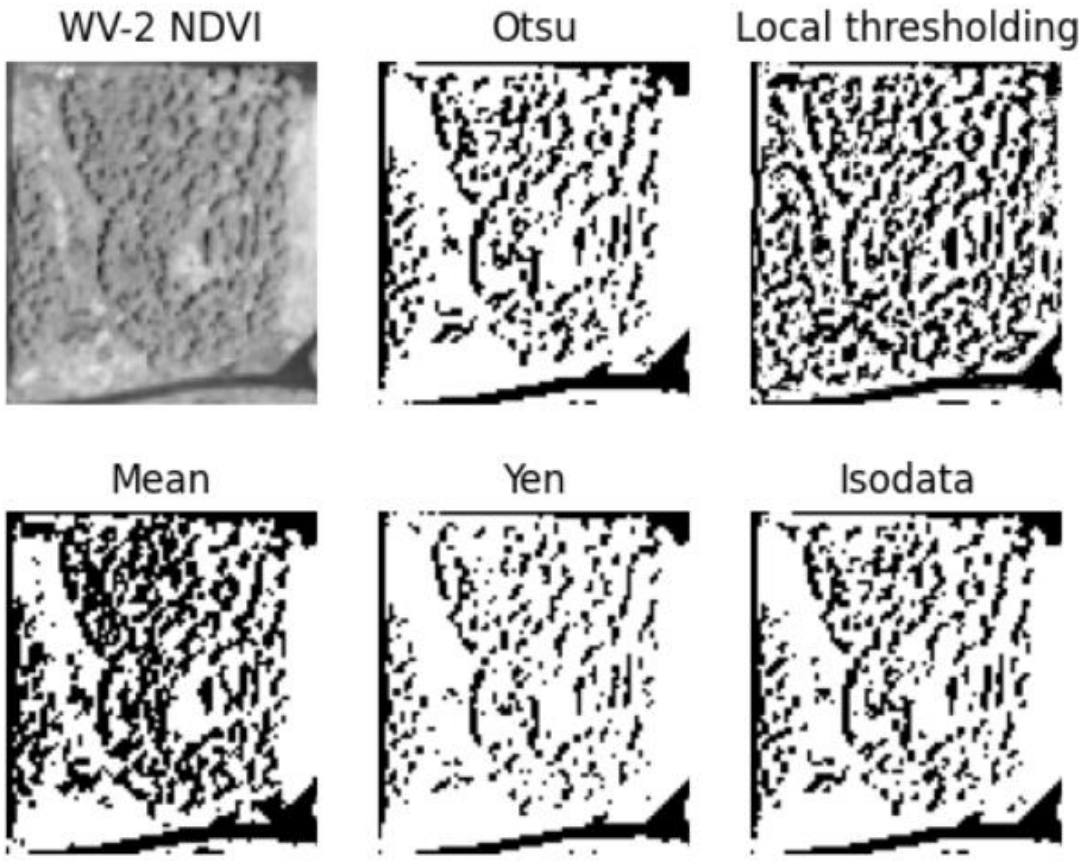

Figure 5.22: WV-2 NDVI Thresholds

Assessment of the accuracy of the threshold algorithms is only applied for Otsu algorithm due to the usage of this method in CD. The manually delineated ground-truth maps were compared with the Otsu results of UAV and WV-2. F-scores of the results are given in Table 5.5.

Table 5.5: Otsu threshold results with respect to ground-truth map with class confusion values and F1- scores. 0: non-vegetation. 1: vegetation

UAV RGB ortho with Otsu	0	1	F1- Scores
0	43	28	0,64
1	2	27	
WV-2 pansharpened with Otsu	0	1	
0	37	29	0,67
1	2	32	

5.6 Change Detection Results

The pan-sharpened WV-2 and GK-1 images and the UAV orthophoto are compared visually for the CD in ArcGIS Pro. Firstly, UAV and WV-2 are compared by visualising in ArcGIS Pro. There are six months of time difference between images which is not much difference to allow the change to happen. Furthermore, the study area is within Akdeniz University campus which may be protected by the university. The seasonal difference can be seen between the images. The bare land in the UAV image was greener in the WV-2 image. The visual comparison between GK-1 and other images were challenging because of the spatial resolution and the amount of shadow that exists in the GK-1 image. Overall, the extent of the area remained unchanged, which is an expected result due to the preservation of the area by Akdeniz University. The change between vegetation and non-vegetation are relatively small. This result could be caused by the variation of methods and platforms.

The CD process was performed by comparing the results of vegetation maps produced with GRVI method by applying the Otsu thresholding algorithm. These images were presented in Figures 5.16, 5.18 and 5.21. The differences were evaluated as unchanged areas and transitions between vegetation (1) and non-vegetation (0) classes. The change ratios as percentages of all pixels in the CD maps are presented in Table 5.6. The CD images between UAV/WV-2 and WV-2/GK-1 are given in Figure 5.26.

Table 5.6: Change ratio in vegetation areas. 1: Vegetation 0: Non-vegetation.

Change Image	1-1	0-0	1-0	0-1	Total
UAV GRVI → WV-2 GRVI	46.1%	28.9%	8.9%	16.1%	100%
WV-2 GRVI → GK-1 PAN	49.0%	22.8%	12.5%	15.7%	100%

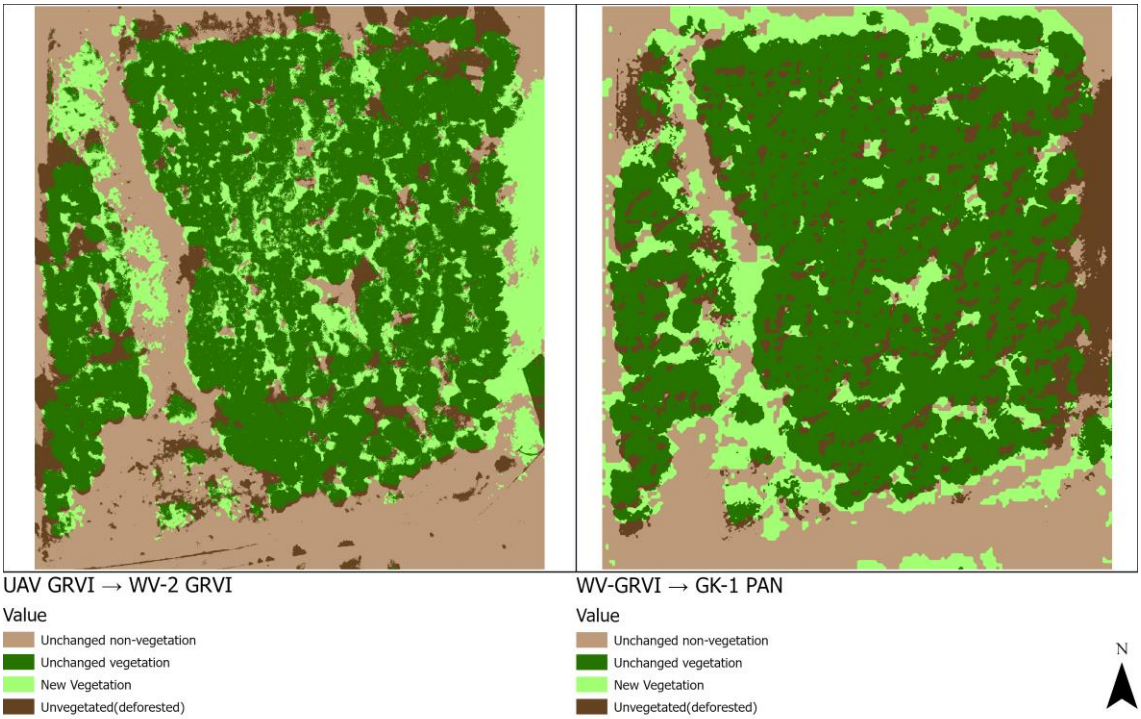

Figure 5.24: CD maps between UAV/WV-2 (left) and WV-2/GK-1 images periods obtained from the pixel-wise comparison of Otsu-thresholded binary GRVI data of all three sensors data.

6. DISCUSSIONS

This study aimed to detect vegetation in different images acquired from the multi-platform, multi-sensor and multi-temporal images in a small forest area over Akdeniz University Campus, and to monitor changes over several years. Many vegetation mapping and classification methods have been investigated and evaluated within the limitations of time and data restrictions of this thesis.

The multi-platform datasets include UAV aerial imagery, WV-2 and GK-1 satellite images obtained at different times. The earliest data was UAV which was obtained in Jan 2015. The following dataset was WV-2 and the acquisition date was May 2015 and the latest dataset, which allows the detect most changes in the study area was obtained in September 2019 from Göktürk-1 satellite. In terms of spatial resolutions, the highest resolution belongs to the UAV dataset as expected which is 1.6 cm GSD for the raw images and 2 cm for orthophoto. The WV-2 dataset involves panchromatic, pan-sharpened and multi-spectral images. The pan-sharpened image and pan images had 0.5 m spatial resolution and considered as VHR in remote sensing. GK-1 pan and pan-sharpened datasets have 1 m spatial resolution while the MS images have 2.5 m spatial resolution.

The study evaluated the potential of the mentioned sensors for vegetation mapping and several supervised and unsupervised methods for this purpose. Satellite and aerial imagery have been used in many studies on several topics including agriculture, urban planning and rural areas. One of the main research topics was if ground-based mapping would leave its place to spaceborne and airborne imagery especially in the field of vegetation mapping. Ground-based methods have their place as auxiliary data nowadays. Satellite imagery and aerial imagery have been used and tested in many types of research both together and separately for obtaining data. Even though UAV offers a great resolution, it lacks sufficient battery power to scan large areas such as forests and crop fields. Furthermore, UAV imagery can be costly for small vegetation communities. Satellite imagery on the other hand can be less costly but offers lower-resolution imagery. High-resolution satellite imagery can be more costly than UAV imagery but can cover a larger area in a short time. Some studies suggest that using both image sources can be

beneficial for small and large vegetation communities. The CD was simply the difference between images and the simplest method has been used in this study.

Based on the research many methods have come across for vegetation mapping and detecting changes. Finding a method that worked on all datasets was challenging. Local maxima and minima, local binary pattern, watershed algorithms, grey-level co-occurrence matrices, vegetation indices, Hough circle, random forest and support vector machine methods were used in many of the researches which have been found during the literature survey. Even though most of these algorithms were evaluated here, some were not presented since the results were not satisfactory. Although implementation issues, which could not be solved in the limited time, were experienced in some cases, the difference that comes with using multi-platform data was the real problem.

WV-2 data was the most efficient among the other datasets used in this study in terms of processing. The pan-sharpened, MS and pan images were filed neatly and there was no more processing needed in order to use the data other than aligning with other datasets. GK-1 dataset file directory, on the other hand, were mixed and it was always difficult the find the image needed at certain times. The original UAV datasets included some 500 images, but the elimination of about 375 images was needed because the images were captured on the same spot which made the processing longer and harder. Also, the images lacked initial georeferencing information which made the processing a bit difficult. Applications like ArcGIS Pro, DroneDeploy, MapWings, MapsMadeEasy and Open Drone Map were not able to process the data because of the missing georeferencing information. It could have been possible to integrate the coordinates into the images using the interior and exterior orientation parameters but that was not possible due to the time limitations. Agisoft Metashape software was able to process the imagery. This part of the processing was the most difficult in terms of preparing the data.

GK-1 and UAV imagery were obtained before noon, which created a problem for analyzing trees because of the shadows that occurred due to the angle of the Sun. The shadows were the main problem in most of the tested methods. Even masking them did not solve the problem for feature extraction because masking was not always possible because of the resolution of the dataset. Furthermore, the more a method requires manual editing the more it lacks efficiency and usability. The geometric accuracy of data is

important because the datasets will be compared with each other and the change between them will be analyzed. Therefore, georeferencing of the datasets was performed meticulously.

Due to the many reasons mention above, vegetation indices were the most useful method of all for feature extraction. Due to the missing NIR band in the UAV dataset, during the literature research, GRVI was found as one of the most used vegetation indices when there was no NIR band in the data. For comparison purposes, GRVI was applied to each dataset. The NDVI was only applied to satellite images. GK-1 GRVI result was one of the most significant result for GK-1 dataset. The lower image resolution and the shadows in the dataset caused difficulties in the determination of vegetation, and the GRVI algorithm enhanced the vegetation information to obtain the most successful results of GK-1 dataset compared to other tested methods in the study.

For image classification, the RF algorithm was chosen because of the frequent use in vegetation mapping. The RF algorithm was used commonly and there were many sources available on Internet. Scikit-learn was the most used machine learning library in Python. The sample algorithms were easy to adapt to the datasets with some minor twists. The classification report in the library was used for the accuracy evaluation. Classes accuracy varied between vegetation and non-vegetation classes. In some cases classes were mixed between each other.

The ground-truth maps were difficult to delineate manually due to several reasons including; image resolution, cursor precision, operator skills, etc.. Nonetheless, ground-truth maps helped the validate the results of Otsu thresholding and RF classification. F1 scores of the classification results were higher in the UAV and WV-2 datasets. This may be caused by the spatial resolution of the datasets.

The CD was applied at decision level by using the best vegetation map obtained from each sensor. Also, the study area was in the University campus and can be considered a protected area. Mainly, the growth of vegetation was observed in time. Here, the CD was carried out in 2D only.

7. CONCLUSIONS AND FUTURE WORK

Overall, this study aimed to identify vegetation using imagery from different platforms. GK-1, WV-2 were spaceborne images and UAV data was airborne images. These datasets varied in temporal, spatial and spectral resolutions, which made the processing of these images together difficult. The geometric processing task was the main step in the data preparation for correct detection of changes. Because of the missing coordinate information in the UAV dataset, the preprocessing of the UAV data required the longest time in processing. With the use of improved direct georeferencing techniques, this time may be shortened. This would also create opportunities in testing and validating many UAV imagery processing software available in the market nowadays.

Within the study, it was concluded that the timing of the image acquisition is crucial for vegetation mapping. Specific purposes like finding vegetation or even counting trees require an image that does not contain any shadow. The off-nadir angle during image acquisition is also an important parameter. It is suggested to use nadir satellite imagery for this purpose.

In UAV imagery, it is suggested to capture images at noon and when there is no wind present to make it easier to identify treetops. In terms of methods, RF has resulted well overall, but further investigation and testing of other machine learning algorithms might be beneficial. The parameterization of RF can be investigation in detail for increasing the classification success as future work. In scikit-learn models, there were many options to modify the applied algorithm and not all of them were entirely tested in this study which can be looked further in the future. On the other hand, although local maxima algorithm has resulted great in most studies, its use could not be exploited fully in this study. The method can be investigated further in the future. Furthermore, local maxima algorithm can be applied to DSM of UAV RGB for tree counting. The GRVI index was found useful for the vegetation detection in RGB images and may even outperform NDVI depending on the image radiometric properties. Otsu thresholding method was utilized for the conversion of GRVI data into a binary vegetation map with vegetated and non-vegetated pixels.

Vegetation indices used in this study were limited to only two indices which are only the tip of the iceberg. There are far more indices available in the literature that can be utilized in future studies. The CD could be applied in feature-level methods instead of decision-level for exploiting the potential of the sensor fusion methods. The results of thesis offers potential for future research on the topic.

REFERENCES

[1] Q. Feng, J. Liu, and J. Gong, "UAV Remote sensing for urban vegetation mapping using random forest and texture analysis," *Remote Sens.*, vol. 7, no. 1, pp. 1074–1094, 2015, doi: 10.3390/rs70101074.

[2] U. C. Benz, P. Hofmann, G. Willhauck, I. Lingenfelder, and M. Heynen, "Multi-resolution, object-oriented fuzzy analysis of remote sensing data for GIS-ready information," *ISPRS J. Photogramm. Remote Sens.*, vol. 58, no. 3–4, pp. 239–258, 2004, doi: 10.1016/j.isprsjprs.2003.10.002.

[3] J. Tigges, T. Lakes, and P. Hostert, "Urban vegetation classification: Benefits of multitemporal RapidEye satellite data," *Remote Sens. Environ.*, vol. 136, pp. 66–75, 2013, doi: 10.1016/j.rse.2013.05.001.

[4] X. Li and G. Shao, "Object-based urban vegetation mapping with high-resolution aerial photography as a single data source," *Int. J. Remote Sens.*, vol. 34, no. 3, pp. 771–789, 2013, doi: 10.1080/01431161.2012.714508.

[5] S. Candiago, F. Remondino, M. De Giglio, M. Dubbini, and M. Gattelli, "Evaluating multispectral images and vegetation indices for precision farming applications from UAV images," *Remote Sens.*, vol. 7, no. 4, pp. 4026–4047, 2015, doi: 10.3390/rs70404026.

[6] A. Voisin, V. A. Krylov, G. Moser, S. B. Serpico, and J. Zerubia, "Supervised classification of multisensor and multiresolution remote sensing images with a hierarchical copula-based approach," *IEEE Trans. Geosci. Remote Sens.*, vol. 52, no. 6, pp. 3346–3358, 2014, doi: 10.1109/TGRS.2013.2272581.

[7] P. A. Burrough, J. P. Wilson, P. F. M. Van Gaans, and A. J. Hansen, "Fuzzy k-means classification of topo-climatic data as an aid to forest mapping in the Greater Yellowstone Area, USA," *Landsc. Ecol.*, vol. 16, no. 6, pp. 523–546, 2001, doi: 10.1023/A:1013167712622.

[8] S. Bhatnagar, L. Gill, S. Regan, S. Waldren, and B. Ghosh, "A nested drone-satellite approach to monitoring the ecological conditions of wetlands," *ISPRS J. Photogramm. Remote Sens.*, vol. 174, no. February, pp. 151–165, 2021, doi: 10.1016/j.isprsjprs.2021.01.012.

[9] T. Wu *et al.*, “Geo-object-based vegetation mapping via machine learning methods with an intelligent sample collection scheme: A case study of taibai mountain, china,” *Remote Sens.*, vol. 13, no. 2, pp. 1–23, 2021, doi: 10.3390/rs13020249.

[10] G. Khadanga and K. Jain, “Tree Census Using Circular Hough Transform and GRVI,” *Procedia Comput. Sci.*, vol. 171, pp. 389–394, 2020, doi: 10.1016/j.procs.2020.04.040.

[11] A. N. Skurikhin, S. R. Garrity, N. G. McDowell, and D. M. Cai, “Automated tree crown detection and size estimation using multi-scale analysis of high-resolution satellite imagery,” *Remote Sens. Lett.*, vol. 4, no. 5, pp. 465–474, 2013, doi: 10.1080/2150704X.2012.749361.

[12] M. A. Wulder, W. A. Kurz, and M. Gillis, “National level forest monitoring and modeling in Canada,” *Prog. Plann.*, vol. 61, no. 4, pp. 365–381, 2004, doi: 10.1016/S0305-9006(03)00069-2.

[13] A. R. Bankert, E. H. Strasser, C. G. Burch, and M. D. Correll, “An open-source approach to characterizing Chihuahuan Desert vegetation communities using object-based image analysis,” *J. Arid Environ.*, vol. 188, no. September, p. 104383, 2021, doi: 10.1016/j.jaridenv.2020.104383.

[14] M. Niphadkar, H. Nagendra, C. Tarantino, M. Adamo, and P. Blonda, “Comparing pixel and object-based approaches to map an understorey invasive shrub in tropical mixed forests,” *Front. Plant Sci.*, vol. 8, no. May, pp. 1–18, 2017, doi: 10.3389/fpls.2017.00892.

[15] J. K. Gilbertson, J. Kemp, and A. van Niekerk, “Effect of pan-sharpening multi-temporal Landsat 8 imagery for crop type differentiation using different classification techniques,” *Comput. Electron. Agric.*, vol. 134, pp. 151–159, 2017, doi: 10.1016/j.compag.2016.12.006.

[16] B. Fu *et al.*, “Comparison of object-based and pixel-based Random Forest algorithm for wetland vegetation mapping using high spatial resolution GF-1 and SAR data,” *Ecol. Indic.*, vol. 73, no. 3–4, pp. 105–117, 2017, doi: 10.1016/j.ecolind.2016.09.029.

[17] N. KAMAGATA, K. HARA, M. MORI, Y. AKAMATSU, Y. LI, and Y. HOSHINO, “A new method of vegetation mapping by object-based classification

using high resolution satellite data," *J. Japan Soc. Photogramm. Remote Sens.*, vol. 45, no. 1, pp. 43–49, 2006, doi: 10.4287/jsprs.45.43.

[18] I. L. Castillejo-González *et al.*, "Object- and pixel-based analysis for mapping crops and their agro-environmental associated measures using QuickBird imagery," *Comput. Electron. Agric.*, vol. 68, no. 2, pp. 207–215, 2009, doi: 10.1016/j.compag.2009.06.004.

[19] T. G. Whiteside, G. S. Boggs, and S. W. Maier, "Comparing object-based and pixel-based classifications for mapping savannas," *Int. J. Appl. Earth Obs. Geoinf.*, vol. 13, no. 6, pp. 884–893, 2011, doi: 10.1016/j.jag.2011.06.008.

[20] X. Zhang, X. Feng, and H. Jiang, "Object-oriented method for urban vegetation mapping using ikonos imagery," *Int. J. Remote Sens.*, vol. 31, no. 1, pp. 177–196, 2010, doi: 10.1080/01431160902882603.

[21] F. Palm, "Urban Vegetation Mapping using Remote Sensing Techniques - A comparison of methods," p. 24, 2015.

[22] S. Ji, C. Zhang, A. Xu, Y. Shi, and Y. Duan, "3D convolutional neural networks for crop classification with multi-temporal remote sensing images," *Remote Sens.*, vol. 10, no. 1, 2018, doi: 10.3390/rs10010075.

[23] L. Zhong, L. Hu, and H. Zhou, "Deep learning based multi-temporal crop classification," *Remote Sens. Environ.*, vol. 221, no. March 2018, pp. 430–443, 2019, doi: 10.1016/j.rse.2018.11.032.

[24] P. Gong *et al.*, "Stable classification with limited sample: transferring a 30-m resolution sample set collected in 2015 to mapping 10-m resolution global land cover in 2017," *Sci. Bull.*, vol. 64, no. 6, pp. 370–373, 2019, doi: 10.1016/j.scib.2019.03.002.

[25] M. Linderman *et al.*, "Using artificial neural networks to map the spatial distribution of understorey bamboo from remote sensing data," *Int. J. Remote Sens.*, vol. 25, no. 9, pp. 1685–1700, 2004, doi: 10.1080/0143116031000159897l.

[26] P. Surovỳ and K. Kuželka, "Acquisition of forest attributes for decision support at the forest enterprise level using remote-sensing techniques-a review," *Forests*, vol. 10, no. 3, 2019, doi: 10.3390/f10030273.

[27] "What is Random Forest? | IBM." [Online]. Available:

https://www.ibm.com/cloud/learn/random-forest.

[28] E. Agrillo *et al.*, "Earth observation and biodiversity big data for forest habitat types classification and mapping," *Remote Sens.*, vol. 13, no. 7, 2021, doi: 10.3390/rs13071231.

[29] P. Das, S. Mudi, M. D. Behera, S. K. Barik, D. R. Mishra, and P. S. Roy, "Automated Mapping for Long-Term Analysis of Shifting Cultivation in Northeast India," *Remote Sens.*, vol. 13, no. 6, p. 1066, 2021, doi: 10.3390/rs13061066.

[30] A. C. Kedia *et al.*, "An Integrated Spectral–Structural Workflow for Invasive Vegetation Mapping in an Arid Region Using Drones," *Drones*, vol. 5, no. 1, p. 19, 2021, doi: 10.3390/drones5010019.

[31] H. Gilani *et al.*, "Evaluating mangrove conservation and sustainability through spatiotemporal (1990–2020) mangrove cover change analysis in Pakistan," *Estuar. Coast. Shelf Sci.*, vol. 249, no. November 2020, p. 107128, 2021, doi: 10.1016/j.ecss.2020.107128.

[32] B. Johnson, "Effects of pansharpening on vegetation indices," *ISPRS Int. J. Geo-Information*, vol. 3, no. 2, pp. 507–522, 2014, doi: 10.3390/ijgi3020507.

[33] A. T. Tran, K. A. Nguyen, Y. A. Liou, M. H. Le, V. T. Vu, and D. D. Nguyen, "Classification and observed seasonal phenology of broadleaf deciduous forests in a tropical region by using multitemporal sentinel-1a and landsat 8 data," *Forests*, vol. 12, no. 2, pp. 1–21, 2021, doi: 10.3390/f12020235.

[34] P. Kempeneers, F. Sedano, L. Seebach, P. Strobl, and J. San-Miguel-Ayanz, "Data fusion of different spatial resolution remote sensing images applied to forest-type mapping," *IEEE Trans. Geosci. Remote Sens.*, vol. 49, no. 12 PART 2, pp. 4977–4986, 2011, doi: 10.1109/TGRS.2011.2158548.

[35] T. Majasalmi and M. Rautiainen, "Representation of tree cover in global land cover products: Finland as a case study area," *Environ. Monit. Assess.*, vol. 193, no. 3, 2021, doi: 10.1007/s10661-021-08898-2.

[36] V. Lawley, M. Lewis, K. Clarke, and B. Ostendorf, "Site-based and remote sensing methods for monitoring indicators of vegetation condition: An Australian review," *Ecol. Indic.*, vol. 60, pp. 1273–1283, 2016, doi: 10.1016/j.ecolind.2015.03.021.

[37] G. Kaplan and U. Avdan, "MAPPING and MONITORING WETLANDS USING

SENTINEL-2 SATELLITE IMAGERY," *ISPRS Ann. Photogramm. Remote Sens. Spat. Inf. Sci.*, vol. 4, no. 4W4, pp. 271–277, 2017, doi: 10.5194/isprs-annals-IV-4-W4-271-2017.

[38] A. Singh, "Review Articlel: Digital change detection techniques using remotely-sensed data," *Int. J. Remote Sens.*, vol. 10, no. 6, pp. 989–1003, 1989, doi: 10.1080/01431168908903939.

[39] L. Bruzzone and F. Bovolo, "A novel framework for the design of change-detection systems for very-high-resolution remote sensing images," *Proc. IEEE*, vol. 101, no. 3, pp. 609–630, 2013, doi: 10.1109/JPROC.2012.2197169.

[40] S. Mishra, P. Shrivastava, and P. Dhurvey, "Change Detection Techniques in Remote Sensing: A Review," *Int. J. Wirel. Mob. Commun. Ind. Syst.*, vol. 4, no. 1, pp. 1–8, 2017, doi: 10.21742/ijwmcis.2017.4.1.01.

[41] D. L. C. Author, P. Mausel, E. Brondízio, and E. Moran, "Change detection techniques," *Int. J. Remote Sens.*, vol. 25, no. 12, pp. 2365–2401, 2004, doi: 10.1080/0143116031000139863.

[42] M. Volpi, D. Tuia, F. Bovolo, M. Kanevski, and L. Bruzzone, "Supervised change detection in VHR images using contextual information and support vector machines," *Int. J. Appl. Earth Obs. Geoinf.*, vol. 20, no. 1, pp. 77–85, 2012, doi: 10.1016/j.jag.2011.10.013.

[43] C. Listner and I. Niemeyer, "Object-based change detection," *Photogramm. Fernerkundung, Geoinf.*, vol. 2011, no. 4, pp. 233–245, 2011, doi: 10.1127/1432-8364/2011/0085.

[44] X. Wang, S. Liu, P. Du, H. Liang, J. Xia, and Y. Li, "Object-based change detection in urban areas from high spatial resolution images based on multiple features and ensemble learning," *Remote Sens.*, vol. 10, no. 2, 2018, doi: 10.3390/rs10020276.

[45] J. Tian, P. Reinartz, P. d'Angelo, and M. Ehlers, "Region-based automatic building and forest change detection on Cartosat-1 stereo imagery," *ISPRS J. Photogramm. Remote Sens.*, vol. 79, pp. 226–239, 2013, doi: 10.1016/j.isprsjprs.2013.02.017.

[46] D. A. Pouliot, D. J. King, F. W. Bell, and D. G. Pitt, "Automated tree crown detection and delineation in high-resolution digital camera imagery of coniferous

forest regeneration," *Remote Sens. Environ.*, vol. 82, no. 2–3, pp. 322–334, 2002, doi: 10.1016/S0034-4257(02)00050-0.

[47] C. Suo, E. McGovern, and A. Gilmer, "Coastal dune vegetation mapping using a multispectral sensor mounted on an UAS," *Remote Sens.*, vol. 11, no. 15, pp. 1–19, 2019, doi: 10.3390/rs11151814.

[48] A. Agarwal, A. K. Singh, S. Kumar, and D. Singh, "Critical analysis of classification techniques for precision agriculture monitoring using satellite and drone," *2018 13th Int. Conf. Ind. Inf. Syst. ICIIS 2018 - Proc.*, no. 978, pp. 83–88, 2018, doi: 10.1109/ICIINFS.2018.8721422.

[49] Z. Szantoi, S. E. Smith, G. Strona, L. P. Koh, and S. A. Wich, "Mapping orangutan habitat and agricultural areas using Landsat OLI imagery augmented with unmanned aircraft system aerial photography," *Int. J. Remote Sens.*, vol. 38, no. 8–10, pp. 2231–2245, 2017, doi: 10.1080/01431161.2017.1280638.

[50] S. Bhatnagar, L. Gill, and B. Ghosh, "Drone image segmentation using machine and deep learning for mapping raised bog vegetation communities," *Remote Sens.*, vol. 12, no. 16, 2020, doi: 10.3390/RS12162602.

[51] C. M. Gevaert, J. Tang, F. J. García-Haro, J. Suomalainen, and L. Kooistra, "Combining hyperspectral UAV and multispectral Formosat-2 imagery for precision agriculture applications," *Work. Hyperspectral Image Signal Process. Evol. Remote Sens.*, vol. 2014-June, no. June, pp. 2–6, 2014, doi: 10.1109/WHISPERS.2014.8077607.

[52] D. Murugan, A. Garg, and D. Singh, "Development of an Adaptive Approach for Precision Agriculture Monitoring with Drone and Satellite Data," *IEEE J. Sel. Top. Appl. Earth Obs. Remote Sens.*, vol. 10, no. 12, pp. 5322–5328, 2017, doi: 10.1109/JSTARS.2017.2746185.

[53] P. C. Gray *et al.*, "Integrating Drone Imagery into High Resolution Satellite Remote Sensing Assessments of Estuarine Environments," *Remote Sens.*, vol. 10, no. 8, 2018, doi: 10.3390/rs10081257.

[54] T. Kattenborn, J. Lopatin, M. Förster, A. C. Braun, and F. E. Fassnacht, "UAV data as alternative to field sampling to map woody invasive species based on combined Sentinel-1 and Sentinel-2 data," *Remote Sens. Environ.*, vol. 227, no.

January, pp. 61–73, 2019, doi: 10.1016/j.rse.2019.03.025.

[55] A. Räsänen and T. Virtanen, “Data and resolution requirements in mapping vegetation in spatially heterogeneous landscapes,” *Remote Sens. Environ.*, vol. 230, no. April, p. 111207, 2019, doi: 10.1016/j.rse.2019.05.026.

[56] G. Kaplan and U. Avdan, “Sentinel-1 and Sentinel-2 data fusion for wetlands mapping: Balikdami, Turkey,” *Int. Arch. Photogramm. Remote Sens. Spat. Inf. Sci. - ISPRS Arch.*, vol. 42, no. 3, pp. 729–734, 2018, doi: 10.5194/isprs-archives-XLII-3-729-2018.

[57] O. Mutanga, E. Adam, and M. A. Cho, “High density biomass estimation for wetland vegetation using worldview-2 imagery and random forest regression algorithm,” *Int. J. Appl. Earth Obs. Geoinf.*, vol. 18, no. 1, pp. 399–406, 2012, doi: 10.1016/j.jag.2012.03.012.

[58] Digital Globe and DigitalGlobe, “THE BENEFITS OF THE EIGHT SPECTRAL BANDS OF WORLDVIEW-2,” no. March, pp. 1–17, 2010.

[59] R. Pu and S. Landry, “A comparative analysis of high spatial resolution IKONOS and WorldView-2 imagery for mapping urban tree species,” *Remote Sens. Environ.*, vol. 124, pp. 516–533, 2012, doi: 10.1016/j.rse.2012.06.011.

[60] S. L. Ustin *et al.*, “Retrieval of foliar information about plant pigment systems from high resolution spectroscopy,” *Remote Sens. Environ.*, vol. 113, no. SUPPL. 1, pp. S67–S77, 2009, doi: 10.1016/j.rse.2008.10.019.

[61] M. A. Cho *et al.*, “Mapping tree species composition in South African savannas using an integrated airborne spectral and LiDAR system,” *Remote Sens. Environ.*, vol. 125, pp. 214–226, 2012, doi: 10.1016/j.rse.2012.07.010.

[62] DigitalGlobe, “Radiometric Use of WorldView-2 Imagery Technical Note 1 WorldView-2 Instrument Description,” no. November, pp. 1–17, 2010.

[63] Satellite Imaging Corporation, “WorldView-2 Satellite Sensor.” https://www.satimagingcorp.com/satellite-sensors/worldview-2/.

[64] N. Demir, “Using UAVs for detection of trees from digital surface models,” *J. For. Res.*, vol. 29, no. 3, pp. 813–821, 2018, doi: 10.1007/s11676-017-0473-9.

[65] F. G. Gultekin, V. O. Atak, M. E. Ayaz, and M. Ari, “Geometric accuracy in satellite imagery: Test methods Göktürk-1 performance evaluation,” *Proc. 9th Int.*

Conf. Recent Adv. Sp. Technol. RAST 2019, pp. 813–819, 2019, doi: 10.1109/RAST.2019.8767793.

[66] P. Boccardo, C. Sandu, A. Ajmar, and F. Perez, "Digital surface models extraction by Göktürk-1 satellite stereo pairs," *Proc. 9th Int. Conf. Recent Adv. Sp. Technol. RAST 2019*, pp. 827–832, 2019, doi: 10.1109/RAST.2019.8767887.

[67] R. Ravanelli, "Orthoimage generation by GÖKTÜRK-1 A test case in Rome," pp. 1–5.

[68] "Göktürk-1 Earth Observation Satellite." https://directory.eoportal.org/web/eoportal/satellite-missions/g/gokturk-1.

[69] General Directorate of Mapping, "General Directorate of Mapping - Küre." https://www.harita.gov.tr/menu/3.

[70] Agisoft, "Agisoft Metashape," [Online]. Available: https://www.agisoft.com/.

[71] Agisoft, "Tutorial (beginner level): Orthophoto and DEM generation with Agisoft PhotoScan Pro 1.1 (with ground controls points)," vol. 1, 2014.

[72] ESRI, "Esri." https://desktop.arcgis.com/en/arcmap/.

[73] S. Van Der Walt *et al.*, "Scikit-image: Image processing in python," *PeerJ*, vol. 2014, no. 1, pp. 1–18, 2014, doi: 10.7717/peerj.453.

[74] J. P. Pereira and B. Koch, "Scikit-image for trees local maxima detection," no. January 2017, pp. 2–5, 2015.

[75] L. P. Coelho, "Mahotas: Open source software for scriptable computer vision," *J. Open Res. Softw.*, vol. 1, no. 1, p. e3, 2013, doi: 10.5334/jors.ac.

[76] "Geeks for Geeks," [Online]. Available: https://www.geeksforgeeks.org/.

[77] L. Breiman, "Random Forests," *Mach. Learn.*, vol. 45, no. 1, pp. 5–32, 2001, doi: 10.1023/A:1010933404324.

[78] J. R. Quinlan, "Induction of decision trees," *Mach. Learn.*, vol. 1, no. 1, pp. 81–106, 1986, doi: 10.1007/BF00116251.

[79] S. Yilmazer and S. Kocaman, "A mass appraisal assessment study using machine learning based on multiple regression and random forest," *Land use policy*, vol. 99, no. June, p. 104889, 2020, doi: 10.1016/j.landusepol.2020.104889.

[80] F. Pedregosa *et al.*, “Scikit-learn: Machine Learning in Python,” *J. Mach. Learn. Res.*, vol. 12, no. 85, pp. 2825–2830, 2011, [Online]. Available: http://jmlr.org/papers/v12/pedregosa11a.html.

[81] Itseez, “Open Source Computer Vision Library.” 2015.

[82] F. Pedregosa *et al.*, “Scikit-learn: Machine Learning in Python,” *J. Mach. Learn. Res.*, vol. 12, no. 85, pp. 2825–2830, 2011.

[83] T. Wood, “F-Score Definition.” https://deepai.org/machine-learning-glossary-and-terms/f-score.

[84] QGIS Development Team, “QGIS Geographic Information System.” 2009.

[85] FAO, “Fra 2015,” 2015.

[86] N. Otsu, “A Threshold Selection Method from Gray-Level Histograms,” *IEEE Trans. Syst. Man. Cybern.*, vol. 9, no. 1, pp. 62–66, 1979, doi: 10.1109/TSMC.1979.4310076.

APPENDIX

APPENDIX 1 – SOFTWARE

```
import ...

im = cv2.imread('iha-grvi.tif')
im = cv2.cvtColor(im, cv2.COLOR_BGR2GRAY)
#im = skimage.filters.gaussian(im, sigma=1, multichannel=False)

# image_max is the dilation of im with a 20*20 structuring element
# It is used within peak_local_max function
image_max = ndi.maximum_filter(im, size=10, mode='constant')

# Comparison between image_max and im to find the coordinates of local maxima
coordinates = peak_local_max(im, min_distance=30)

# display results
fig, axes = plt.subplots(1, 3, figsize=(8, 3), sharex=True, sharey=True)
ax = axes.ravel()
ax[0].imshow(im, cmap=plt.cm.gray)
ax[0].axis('off')
ax[0].set_title('Original')

ax[1].imshow(image_max, cmap=plt.cm.gray)
ax[1].axis('off')
ax[1].set_title('Maximum filter')
```

Figure A.1: Scikit-Image Local Maxima [73]

```python
# importing required libraries
import mahotas
import mahotas.demos
from pylab import gray, imshow, show
import numpy as np
import matplotlib.pyplot as plt
import cv2

# loading image
img = cv2.imread("test.tif")

# filtering image
img = img.max(2)
print("Image")

# showing image
imshow(img)
show()

# getting local minima of the image
new_img = mahotas.locmin(img)

# showing image
print("Local Minima")
imshow(new_img)
show()
```

Figure A.2: Mahotas Local Minima Code [76]

```
import ...
img = cv2.imread('iha_grvi.tif')

training_labels = np.zeros(img.shape[:2], dtype=np.uint8)
training_labels[450:500, 682:800] = 1
training_labels[400:450, 180:240] = 1

training_labels[340:415, 757:847] = 2
training_labels[780:840, 500:600] = 2

sigma_min = 1
sigma_max = 16
features_func = partial(feature.multiscale_basic_features,
                        intensity=True, edges=False, texture=True,
                        sigma_min=sigma_min, sigma_max=sigma_max,
                        multichannel=True)
features = features_func(img)
clf = RandomForestClassifier(n_estimators=50, n_jobs=-1,
                             max_depth=10, max_samples=0.05)
clf = future.fit_segmenter(training_labels, features, clf)
result = future.predict_segmenter(features, clf)

fig, ax = plt.subplots(1, 2, sharex=True, sharey=True, figsize=(9, 4))
ax[0].imshow(segmentation.mark_boundaries(img, result, mode='thick'))
ax[0].contour(training_labels)
ax[0].set_title('Image, mask and segmentation boundaries')
ax[1].imshow(result)
ax[1].set_title('Segmentation')
fig.tight_layout()
plt.show()
```

Figure A.3: Random Forest Classifier code for the UAV image [80]

```
from skimage.filters import threshold_otsu, threshold_local, \
    threshold_isodata, threshold_mean, threshold_yen
import matplotlib.pyplot as plt
import cv2

image = cv2.imread('iha-grvi.tif')
image = cv2.cvtColor(image, cv2.COLOR_BGR2GRAY)

global_thresh = threshold_otsu(image)
otsu = image > global_thresh

global_thresh = threshold_isodata(image)
isodata = image > global_thresh

global_thresh = threshold_mean(image)
mean = image > global_thresh

global_thresh = threshold_yen(image)
yen = image > global_thresh

block_size = 35
local_thresh = threshold_local(image, block_size, offset=10)
local = image > local_thresh
```

Figure A.4: Scikit-Image histogram sample code [73]

CIRRICULUM VITAE